Centre for Geo-Information

Thesis Report GIRS-2004-24

CONTRIBUTION OF SURFACE ENERGY BALANCE SYSTEME (SEBS) TO PRODUCE THE CLIMATOLOGY OF EVAPOTRANSPIRATION FOR THE NETHERLANDS

Raoul A. Adjobo

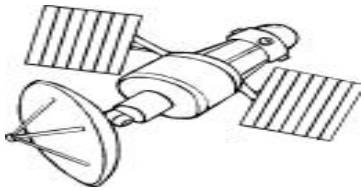

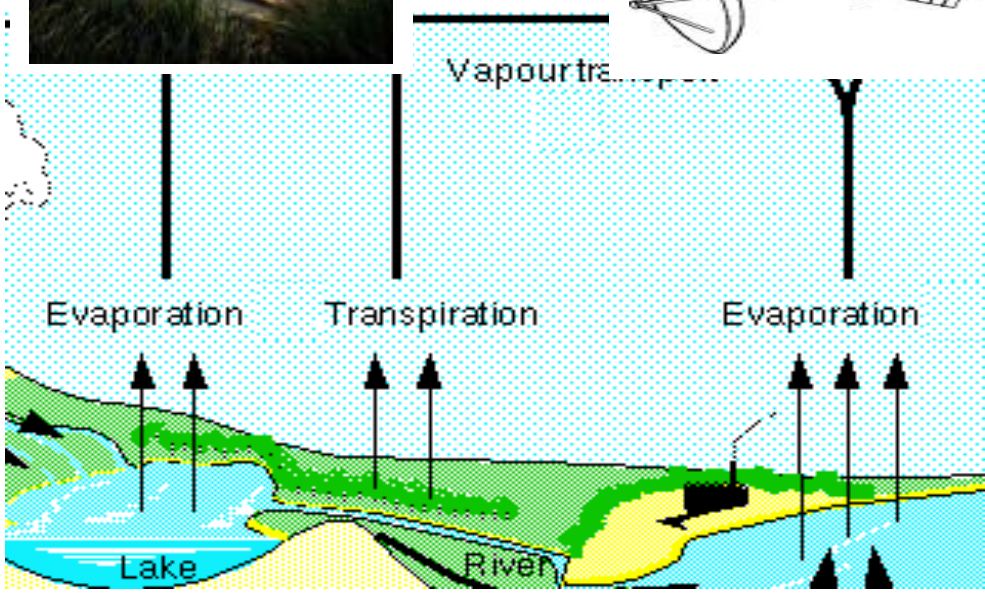

April 2004

WAGENINGEN UNIVERSITY
WAGENINGEN UR

CONTRIBUTION OF SURFACE ENERGY BALANCE SYSTEME (SEBS) TO PRODUCE THE CLIMATOLOGY OF EVAPOTRANSPIRATION FOR THE NETHERLANDS

by

Raoul A. Adjobo

Registration number 73-01-01-005-010

Degree Assessment Board:

Dr. Ir. Bob Z. Su
First supervisor
Dr. Ir. Jan Clevers
Second supervisor
Dr. Ir. Sytze de Bruin
External Examiner

A thesis submitted in partial fulfilment of the requirements for the degree of Master of Science at Wageningen University and Research Centre, The Netherlands.

April 2004
Wageningen, The Netherlands

Thesis code number: GRS-80326
Wageningen University and Research Centre
Laboratory of Geo-Information Science and Remote Sensing
Thesis Report: GIRS-2004-24

Acknowledgments

First of all, I would like to address my specific gratitude to the Dutch Government, my sponsor for this MSc study at Wageningen University, who provided me with a grant to cover all the study expenses.

My deep thanks to my supervisors Dr. Ir. Bob Z. Su & Dr. Ir. Jan Clevers to have put their time, already too charged by their daily work, and their energy at my profit. Thank you to have supervised, have directed and have led this work to the end.

Specific thanks to Prof Li Wan from China, who came to solve my software difficulties and help me by that to be able to run the SEBS program in a proper way and get some results.

I will never finish enough thanking Dr. Gerbert Roerink, Drs. Allard de Wit, Drs. Harm Bartholomeus for their availability, their promptitude and their willingness to carry me assistance and to discuss all the technical aspects of this work with me so to improve its quality.

My gratitude go to Mr. Han Stricker who has spontaneously accepted to stigmatize the insufficiencies and to bring constructive criticisms to this work.

Thank you Piet Warmerdam and Jacques Kole to have provided me with data for the validation for this work.

To all those, in one way or another, who have contributed to my selection for this master and/or have contributed to my formation here at Wageningen University and Research Centre, from my study director to my professors while going through my study adviser and all the administrative staff of the university, I address big thanks.

At last but not the least, I would like, here and now, to testify all my gratitude and my recognition with my wife and my mother-in-law and through them with all my family-in-law's members here in the Netherlands who supported me morally, financially as well as materially in all the steps having led to the end to this master degree.

Abstract

For this study, we made use of 15 years AVHRR_1b images along with meteorological data, respectively from NOAA and KNMI archives as input into the SEBS algorithms (SEBS GUI V3.3) to derive the daily evaporation of about 145 days during the period between 1989 and 2003. The robustness and accuracy of our generated results were validated against KNMI measured data of the same days as our images. A large discrepancy was found between the two. We attempted to understand this difference by checking the main input data and our preliminary results. There, we came up with the remarks that the SEBS method underestimates some intermediary results such as NDVI and albedo during the growing season. These parameters are used several times in successive steps of the processing and lead to a propagation and an accumulation of errors. Furthermore, the derivation of these intermediary results and their accuracy depend on the accuracy of the preliminary input data like surface roughness height (z_0), surface resistance (r_s) and the aerodynamic resistance (r_a) over heterogeneous landscapes consisting of a mix of low and high vegetation, open water and urban areas. Thus, we conclude that the major challenge for the improvement and successfulness of the SEBS algorithms lies on the development of a method for estimating the aerodynamic surface variables using remote sensing techniques and the accurate estimation of the surface fluxes. Future researches have to be done in that sphere along with better calibration and parameterization to make SEBS usable all over the world and under all climate conditions.

Key words:
AVHRR_1b images, meteorological data, daily evaporation, SEBS algorithms, remote sensing, NDVI, albedo, surface roughness height, aerodynamics resistance, surface fluxes.

CHAPTER 1: GENERAL INTRODUCTION

1.1. Research background

Without the continued circulation of water through the environment (referred to as the hydrological cycle), much of the life on Earth would cease (Jackson & Jackson, 1998). This is because water plays many roles in the sustenance of life including the maintenance of a world climate that is compatible with continued life. Indeed, through the processes of evaporation and transpiration, water traps and redistributes a significant proportion of the solar energy arriving at the earth surface. About 22% of the solar radiation absorbed by the Earth drives the water cycle (Owen *et al.*, 1998). This energy causes the water to move by evaporation from the oceans, rivers, plants, etc. into the atmosphere, whence it is eventually deposited as rainfall (precipitation), or snow.

The process by which water changes phases from liquid to gas is called evaporation and may take place directly from streams, oceans, moist soil, and wet vegetation (Owen *et al.*, 1998). Thus, the atmosphere surrounding the earth soaks up water. The capacity of the atmosphere to hold water vapor defines the air humidity gradient. Under certain conditions, the water molecules contained in the air move and collect into liquid phase (condensation) and form clouds (http://faldo.atmos.uiuc.edu/w_unit/LESSONS/water.cycle.html). The clouds fall as precipitation (rain, snow, hail and so on) when they become so large that the wind cannot keep them in the sky. The evaporation is controlled, among other factors, by the heat available, the degree of saturation of the air, and the wind speed.

Transpiration is defined as the loss of water from the leaves and other aerial parts of the plants (Jackson & Jackson, 1998). Water vapor mainly escapes from the surface of the leaves through pores (stomata). It occurs mainly during the process of green plant's photosynthesis. Transpiration is important for plants' survival since it pulls water up from the roots to supply photosynthesis, to bring minerals from the roots for biosynthesis within the leaf and to cool the leaf (http://users.rcn.com/jkimball.ma.ultranet/BiologyPages/T/Transpiration.html). Thus, transpiration occurs in all vegetation and its rate may differ according to the time of the day or of the year and the vegetation growth stage. Transpiration is strongly influenced

by ambient atmospheric conditions; for example high temperatures increase transpiration whilst high humidity decreases it.

In clear conditions, land to atmosphere transfer of moisture is brought about by a combination of evaporation and transpiration through the solar energy and meteorological conditions. These transfers are frequently lumped together and given the term of "evapotranspiration". Surface vegetation and land use play extremely important roles in surface energy fluxes. Plants absorb and reflect solar radiation and also take up water and expel water vapor. The type of plant material, its growth stage and color determine whether and to what extent the surface and air can couple and exchange energy (http://www.arm.gov/docs/sites/sgp/news/sgpfacility/oct00.pdf). The absorption of solar energy at the Earth's surface provides a source of heat that warms the atmosphere from below. This gives the energy that is responsible for driving the weather and climate patterns of the globe.

Problems related to water resource and irrigation management require a reliable estimate of evapotranspiration (Rauwerda *et al.*, 2002)). These estimates, while being founded on a physical basis, should be acquired by as little input variables as possible, preferably no more than meteorological data. By developing the concept of surface energy balance system (SEBS) through remote sensing techniques in the last few years, Alterra Green World Research largely satisfied these requirements. The algorithms derived from this concept attempt to fully understand the partitioning of the incoming solar energy on the Earth surface into its essential components. These components consist of radiative and non-radiative energy. Incoming and outgoing short wave and long wave radiation resulting in a net total radiation (R_n) form the radiative energy balance on the earth while energy used to heat soil (G_o) or air (H) and to evaporate water (λE) constitute the non-radiative part. SEBS algorithms state that radiative and non-radiative fluxes are in balance. Furthermore, it is acknowledged, within the SEBS concept, that the relative partitioning of the available energy into the different fluxes is to a large degree determined by the availability of water or water vapor.

Recently, some studies have been carried out either to use or to validate the SEBS algorithms in China, in the Netherlands, and in Spain. Su *et al.* (2001a) used the SEBS algorithms to develop a methodological way in order to retrieve land physical

parameters. Li (2001) applied SEBS to the Urumuqi river basin in northwest China to derive evapotranspiration for 1995 and validated the results with *in-situ* lysimeter data. Sintonen *et al.* (2002) validated the SEBS algorithms against field data from the Netherlands. Su (2002) and Rauwerda *et al.* (2002) used the SEBS algorithms respectively to estimate the turbulent heat for the Netherlands and the evaporative fraction for Spain and the Netherlands. Su *et al.* (2003a) used SEBS algorithms to derive a technique for drought monitoring in China. These studies on short-term processes yield enough confidence in SEBS algorithms to use them to generate a composite of day-to-day evapotranspiration over a longer period (climatology of evapotranspiration) for the Netherlands as described in this thesis report.

1.2. Problem definition

Nowadays, meteorologists are able to forecast with high precision the expected weather in terms of temperature, precipitation, wind, and solar radiation. Science and technology improvements help to clearly define the global pattern of the world climate and master its influence on our daily lives. One still wishes an accurate estimation of the evaporation and transpiration on a global scale as well as on a local scale. In that perspective, some attempts were made proposing a range of formulas for estimation of evapotranspiration. Among others, we can consider the work of De Bruin & Stricker (2000), which aims to summarise the behaviour of various formulas for evapotranspiration of grass under non-restricted soil moisture conditions in the Netherlands. That publication revised the methods of Makkink, Priestley-Taylor, Penman, Penman-Monteith, Thom-Oliver and FAO to conclude on the practicability and attractiveness of Makkink 's method which justified its use by KNMI since 1987 and furthermore came up with the result that "evaporation is primarily determined by the available energy (i.e. net radiation minus the soil heat flux density (R_n-G_o))". These findings support SEBS basic and driving concepts namely that the precise quantification of evaporation, through remote sensing techniques, is mainly possible under a better understanding of the surface energy partitioning into its components at the land surface. Indeed, an integration of remote sensing and image processing in estimating evapotranspiration data can decrease the costs, reduce the time required to capture the data and increase the detail of information. The precise quantification of evaporation provides a wealth of information to water management and hydrology as part of the water runoff process, to agriculture and to nature conservation and environmental issues on plants water stress or drought index as

well as for meteorology and many related fields. Sintonen *et al.* (2002) argued already that: “SEBS can be extended to estimate the actual evaporation, soil water availability and drought stress of agricultural crops”. […]
Furthermore, the estimation of evaporation is, among other domains, used to predict thermal pollution in rivers and for air pollution control (de Bruin, 1998). Moreover, the relevance of this research for society is found, among others, in the area of prevention of climate risk impacts on socio-economical life.

To ensure that our water supply, agricultural system, and nature conservation issues are secure, it might be essential that meteorologists include the prediction of the variation in evaporation and transpiration processes as part of the weather forecasting. Then extreme values (lowest and highest) in a predefined scale can give alarm for setting appropriate measures at the right time. For instance, the most efficient water conservation measures, while allowing better management of water both spatially and temporally, may focus on evapotranspiration quantification and lead to flood control or drought prevention. Scientists define drought, in a broad sense, in relation to the long-term average condition of the balance between precipitation and evapotranspiration in a particular area. In addition, it is recognized that a warmer earth surface will increase evaporation along with the intensity of water cycling, because the greater availability of solar radiation during the daytime enhances the evapotranspiration process. Thus, the intensity and the frequency of extreme events like flooding may increase. Flooding and severe drought are of a critical threat for human beings. One has in mind the recent disaster created by the August 2002 flooding in Europe (Germany and Austria). In the same perspective, Europe has experienced in 2003 one of its hottest and driest summers since 1976 with an estimate of deaths related to the drought of more than 10,000 people in France and many hectares of forest areas and nature destroyed by fire in France, Italy, Portugal and Spain. The invoice of these disasters is a few billion euros. In the Netherlands, the last summer drought and its recurrent high evaporation from the surface water lead to an increase of water salt content and some dikes (like in the IJsselmeer) were opened to reverse this tendency and safeguard the aquatic ecosystem. Also the high level of evaporation has seriously disturbed the river transport of the river channels of the Netherlands and has negatively affected the national economy.

This testifies, if still needed, the relevance and importance of our research for Europe and the Netherlands.

The convictions of the aforementioned relevancy together with the data availability (both NOAA and meteorological data), the possibility to compare our outcome with the Dutch meteorological institute (KNMI) measurements are the main reasons, which justified the choice of the Netherlands as the research area. If successfully accomplished, the same methodology we use for this study can be applied in other areas in the world.

1.3. Research objectives

Quantitative understanding of the processes responsible for land-atmosphere exchange of mass and energy was ascertained by establishing the SEBS algorithms. These algorithms allowed calculating the evaporation (or evaporative fraction) at regional scale with help of pre-established mathematical models. Considering these assets, the overall objective of our research is to develop a method to generate a long-term data set of evapotranspiration for the Netherlands.
By achieving the specific objectives discussed hereafter, it should be possible to contribute more effectively to the further validation of the theory on the surface energy balance algorithms while creating a strategy to be used in water management and conservation:

i) assess the extent at which an accurate net radiation partitioning through SEBS can lead to the generation of evapotranspiration on a daily basis for the Netherlands (mid-latitude);
ii) validate the generated evapotranspiration dataset against KNMI field measurements;
iii) investigate whether and to what extent (nationwide mean or stations based mean) the climatologic dataset generated is sensitive to specific SEBS parameters (NDVI, albedo, T_s-T_a or G_0);
iv) investigate at what extent a better accuracy of SEBS partitioning can be met for the estimation of evapotranspiration (how to improve SEBS and calibrate its functionalities such that reasonable maps of evapotranspiration can be developed for use in water management and planning).

1.4. Research issues

The central research question we would like to answer during this project is: What are the practical issues for evaporation quantification and the use of SEBS to produce evapotranspiration datasets for the Netherlands? In other words, is the SEBS method as accurate as the KNMI one for evapotranspiration prediction or estimation? What are the weaknesses and strong points of SEBS compared to other methods?

Trying to make this main research question more operational regarding the formulated objectives, we come up with the following six sub-questions that, through answering, should contribute to a better understanding of the surface energy balance system.

As specifically related to objective (i):

- While using the SEBS algorithms, can climatological data be assessed and with what precision?

As specifically related to objective (ii):

- What are the similarities and differences between field measured data and predicted data by the SEBS algorithms?
- What explains the differences if there are any?

As specifically related to objective (iii):

- What is the variability of generated evaporative datasets regarding the sensible heat?
- What is the variability of generated evaporative datasets regarding the latent heat?

As specifically related to objective (iv):

- Which level of accuracy in long-term evaporative datasets can be obtained by an improvement in SEBS variables?

1.5. Organization of the thesis

After this chapter of general introduction, chapter 2 follows wherein the concept and theory of the SEBS algorithms developed by Su (2000) and used a number of times already, are briefly presented according to literature. Chapter 3 introduces the procedures of data acquisition (NOAA/AVHRR data and meteorological data) and then

the general methodologies of calculation of evaporation using these data through the SEBS algorithms in the ENVI package. Chapter 4 starts with the presentation of the main results through some image samples, graphs and tables of analysis and ends up with the validation of our process results through its comparison with climatologic stations data (KNMI measured data). Conclusions and recommendations for future research and improvement of the SEBS procedures are presented in chapter 5.

CHAPTER 2: SURFACE ENERGY BALANCE SYSTEM (SEBS): CONCEPT AND THEORY FROM LITERATURE

2.1. The energy balance terms at the Earth's surface

Dr Su and colleagues of the Alterra Green world research of Wageningen University & Research Centre have developed the Surface Energy Balance System (SEBS) concept and algorithms (Su, 2002 and Su *et al.* 1998, 2001b, 2003b). SEBS uses the combination of remote sensing data obtained in the visible and infrared wavelength ranges with meteorological data to estimate land surface turbulent flux and relative evaporation at different scales. In the scope of this thesis, only the main lines of the SEBS theory will be presented, the interested reader may refer to the afore mentioned literature for more details.

2.1.1. Two ways Net Radiation (R_n)

Exchange processes between land surface and its surrounding envelope of gas (i.e. atmosphere) are mainly driven by solar energy. The net radiation or the available energy at the Earth surface is given by:

$$R_n = (1 - \alpha)\, K^{\downarrow} + \varepsilon . L^{\downarrow} - \varepsilon\, \sigma T_o^4 \qquad \text{(eq. 2.1)}$$

where α is the albedo i.e. the reflectance at the land surface as a factor; $K^{\downarrow}$ and $L^{\downarrow}$ are respectively the incoming short and long wave energies from the sun and the atmosphere per unit time per unit surface (in Wm^{-2}); ε is the emissivity of the soil; σ is the Stefan Bolzmann's constant and T_o (in K) is the soil temperature.

At the Earth surface, this net radiation is mainly transformed into three different forms of energy. A part is used to heat up the soil, termed *Soil Heat flux (G_o)*; a part is used to warm up the air above the soil, termed *Sensible Heat flux (H)*. The third part of the net radiation is used to evaporate water into the atmosphere. This energy is obtained by the product of the latent heat of evaporation (λ) and the amount of water evaporated (E) and is termed *Latent Heat flux (λE)*.

Of course part of the available energy is used for the formation of the bio-matter (photosynthesis) but this is ignored here because it is usually very small and can be neglected while compared to the other three forms.

Thus, the net radiation can be rewritten as:

$R_n = G_o + H + \lambda E$ (eq. 2.2)

In a steady state (which we assume to occur in general and thus is our main basic hypothesis for the SEBS theory), eq. 2.1 must equal eq. 2.2 and give the energy balance concept.

2.1.2. The Soil Heat flux (G_o)

The amount of available energy used to warm up the ground is parameterized by the following equation:

$G_o = R_n . [\Gamma_c + (1 - f_c) . (\Gamma_s - \Gamma_c)]$ (eq. 2.3)

Here Γ_c is the ratio of soil heat flux to net radiation taken as a fixed value of $\Gamma_c = 0.05$ for full vegetation canopy (Montheith, 1973) and as a fixed value of $\Gamma_s = 0.315$ for bare soil (Kustas & Daughtry, 1989). An interpolation is thus performed between these limiting cases (full vegetation canopy and bare soil) using the actual fractional canopy coverage, f_c.

2.1.3. Turbulence and bulk approach to determine friction velocity (u), Sensible Heat flux (H) and Obukhov stability length (L)

Different layers of gas form the atmosphere of which the closest to the land surface is called the troposphere. That troposphere can again be divided into a number of layers. Land surface to atmosphere exchange processes which sustain the surface energy balance concept mainly occur in the Atmospheric or Planetary Boundary Layer (PBL) which is defined by Stull (1999) as "the part of the atmosphere that is directly influenced by the underlying surface and responds to surface forcing with a timescale of about an hour or less". De Bruin (1998) estimated the depth of the PBL, according to the meteorological condition, from a few hundred meters to a few kilometers. In this study, we use a fixed value of 1000 m as reference height. Within the bottom 10% of the PBL called the Atmospheric Surface Layer (ASL), irregular airflow (irregular in direction and velocity) governs the motion of matter and thus generates turbulence (Rauwerda *et al.*, 2002). During daytime, available energy partly warms the earth's surface and causes

warm air bubbles to rise, which are replaced by cool air moving downwards. This repeated phenomenon in the ASL sustains the relationships between the profile of the mean wind speed (u) and the mean difference between the soil and the air temperature (θ_o - θ_a). Those two parameters are usually assessed by a bulk parameterization based on Monin-Obukhov Similarity (MOS) theory in modeling energy and mass transfer between land surface and atmosphere and are usually written in the following integral forms:

$$u = \frac{u_*}{k}\left[\ln\left(\frac{z-d}{z_{0m}}\right) - \psi_m\left(\frac{z-d}{L}\right) + \psi_m\left(\frac{z_{0m}}{L}\right)\right] \quad \text{(eq. 2.4)}$$

$$\theta_0 - \theta_a = \frac{H}{ku_*\rho C_p}\left[\ln\left(\frac{z-d}{z_{0h}}\right) - \psi_h\left(\frac{z-d}{L}\right) + \psi_m\left(\frac{z_{0h}}{L}\right)\right] \quad \text{(eq. 2.5)}$$

with z is the height above the surface; $u_* = (\tau_o/\rho)^{1/2}$ the friction velocity; τ_o the surface shear stress; ρ the density of air; k = 0.4 von Karman's constant; d the zero plane displacement height; z_{om} the roughness height for momentum transfer, i.e. the extent at which a surface can generate turbulence or the height above the earth surface at which the wind speed becomes zero; θ_o and θ_a respectively the potential surface and air temperature at the height z; z_{oh} the scalar roughness height for heat transfer, i.e. the capacity of a surface to heat up the PBL due to the surface's radiometric temperature; ψ_m and ψ_h the stability correction function for momentum and sensible heat transfer respectively; L the Obukhov length defined as :

$$L = -\frac{\rho C_p u_*^3 \theta_v}{kgH} \quad \text{(eq. 2.6)}$$

Where g is the acceleration due to gravity; θ_v is the potential virtual temperature near the surface.

The set of equations from 2.4 to 2.6 enables the estimation of sensible heat flux (H) within the ASL and generally is referred to as the Monin Obukhov Similarity Theory. The advantage of this theory is that the derivation of the sensible heat flux requires only

the wind speed and temperature at the reference height as well as the surface temperature and these are independent of other SEBS terms.

2.1.4. The latent heat flux (λE) and the relative evaporation

Once the net radiation, the soil heat flux and sensible heat flux are known, one can derive the latent heat as a residual term from the surface energy balance equation (eq. 2.2). Thus the latent flux is expressed as:

$$\lambda E = R_n - G_o - H \qquad \text{(eq. 2.7)}$$

Since the computation of the sensible heat flux is a function of ground measurements namely wind speed and air temperature, the uncertainties in those observed data cause an error in the latent heat flux. SEBS algorithms constrain this error in a range based on the computation of the sensible heat flux in the extreme wet and dry conditions. In fact the characteristics of the sensible heat flux in the extreme dry and wet conditions obviously enhance the reliability of the computed results.
In the extreme dry condition, the latent heat flux or evaporation will become zero (no evaporation) due to the soil water content that became zero and the following equation can be derived from (eq. 2.7):

$\lambda E_{dry} = R_n - G_o - H_{dry} \equiv 0$, or

$$H_{dry} = R_n - G_o \qquad \text{(eq. 2.8)}$$

In the extreme wet condition, the actual evaporation will be equal to the potential evaporation entirely determined by atmospheric conditions. Then the sensible heat flux achieves its minimum.

$\lambda E_{wet} = R_n - G_0 - H_{wet}$ or

$$H_{wet} = R_n - G_0 - \lambda E_{wet} \qquad \text{(eq. 2.9)}$$

Under those conditions, the relative evaporation will be:

$$\Lambda_r = \frac{\lambda E}{\lambda E_{wet}} = 1 - \frac{\lambda E_{wet} - \lambda E}{\lambda E_{wet}} \qquad \text{(eq. 2.10)}$$

After some algebra, by combining (eq.2.2), (eq. 2.8), (eq. 2.9) and (eq. 2.10), we arrive to the (eq. 2.11) which expresses best the relative evaporation:

$$\Lambda_r = 1 - \frac{H - H_{wet}}{H_{dry} - H_{wet}} \qquad \text{(eq. 2.11)}$$

where H is the actual sensible flux, defined by (eq. 2.5); H_{dry} is the sensible heat flux at the dry limit, given by (eq. 2.8). The sensible heat flux at the wet limit, H_{wet}, is derived by combining (eq. 2.9) with the widely used Penman-Monteith equation.

The properties of the state of flow in the atmosphere namely vapor pressure (e), saturated water vapor pressure (e_w), air and surface temperatures (T_a and T_o), internal and external resistances (r_i and r_e), are integrated in the Penman-Monteith equation for estimation of evaporation and shown in the following formula:

$$\lambda E = \frac{\Delta \cdot r_e (R_n - G_0) + \rho C_p (e_w - e)}{r_e (\gamma + \Delta) + \gamma \cdot r_i} \qquad \text{(eq. 2.12)}$$

with e and e_w vapor pressure and saturated vapor pressure respectively; γ the psychometric constant; Δ the rate of change of saturation vapor pressure as a function of temperature; r_i and r_e respectively the bulk surface internal resistance and the external or aerodynamic resistance.

In practice, some difficulties exist to evaluate latent heat flux due to the fact that the internal resistance, r_i, is generally regulated by the internal surface moisture availability which in turn is influenced by evaporation. So, the direct computation of latent heat flux using r_i is not recommended.

For the completely wet land surface, it is assumed, according to literature, that $r_i = 0$ and according to (eq. 2.9) and (eq. 2.12), the heat flux for the wet condition can be written as follows:

$$H_{wet} = \frac{R_n - G_0 - \frac{\rho C_p (e_w - e)}{r_{ew} \cdot \gamma}}{1 + \Delta/\gamma} \qquad \text{(eq.2.13)}$$

where the external resistance in the extreme wet condition, r_{ew}, is:

$$r_{ew} = \frac{1}{k u_*}\left[\ln\left(\frac{z-d}{z_{0h}}\right) - \psi_h\left(\frac{z-d}{L_w}\right) + \psi_h\left(\frac{z_{0h}}{L_w}\right)\right] \qquad \text{(eq. 2.14)}$$

Under the same condition, the stability length is:

$$L_w = -\frac{\rho u_*^3 \theta_v}{kg \times 0.61 \cdot \left(\frac{R_n - G_0}{\lambda}\right)} \qquad \text{(eq. 2.15)}$$

Once H_{wet} has been determined, the relative evaporation, Λ_r, formulated in (eq. 2.11) can be derived as well as the latent heat flux, λE.

2.2 Surface resistance to heat transfer: model for z_{oh} determination

Surface relief and vegetation structure in a given area mainly control the wind speed (u) and the mean soil-air temperature gradient (θ_o - θ_a), which govern turbulence and aerodynamic parameter values. These unknown variables are needed in (eq. 2.4), (eq. 2.5) and (eq. 2.14) respectively in form of the height displacement d, the roughness for momentum (z_{om}) and heat (z_{oh}) transfer. Massman (1997) proposed a within canopy turbulence model to estimate the aerodynamic parameters, the displacement height, d, and the roughness height for momentum, z_{om}. Su *et al.* (2001b) have shown the reliability of that model compared to the one of Brutsaert (1982) and Wieringa (1986, 1993) quoted by Li (2001) due to the fact that the aerodynamic parameters depend on wind speed and direction besides the surface characteristics. Usually there is a relationship between z_{om} and z_{oh} which is expressed as the kB^{-1} factor:

$$kB^{-1} = \ln\left(\frac{z_{0m}}{z_{0h}}\right) \qquad \text{(eq.2.16)}$$

where B^{-1} is the inverse of the Stanton number, a dimensionless heat transfer coefficient. In SEBS, the model proposed by Su *et al.* (2001b) is used to estimate the kB^{-1} factor. An advantage of that model is that it takes into account the density of roughness elements and the drag exerted by the vegetation elements. The model that integrates simultaneously the contribution of the canopy, of the canopy-soil interaction and of the soil in the aerodynamic estimation, is given as:

$$kB^{-1} = \frac{kC_d}{4C_t \frac{u_*}{u(h)}\left(1 - e^{-n/2}\right)} f_c^2 + f_c f_s \frac{\frac{ku_*}{u(h)}\frac{z_{0m}}{h}}{C_t^*} + kB_s^{-1} \cdot f_s^2 \qquad \text{(eq.2.17)}$$

with f_c the fractional canopy coverage and f_s its compliment. C_d the drag coefficient of the foliage elements assumed to take the value of 0.2; C_t is the heat transfer coefficient of the leaf taken as 0.01; C^*_t is the heat transfer coefficient of soil given by $C_t^* = (0.71)^{-2/3}\,\mathrm{Re}_*^{-0.5}$;

$\mathrm{Re} = \frac{h_s u_*}{\nu}$ is the roughness Reynolds number with h_s the roughness height of soil.

The kinematics viscosity of the air is given by $\nu = 1.327 \cdot 10^{-5}\left(\frac{P_0}{P}\right)\left(\frac{T}{T_0}\right)^{1.81}$ (Massman, 1999 quoted by Li, 2001) with P and T the ambient pressure and temperature; P_o = 101.3 kPa and T_o = 273.15 K.

For a bare soil surface, kB^{-1}_s is calculated according to Brutsaert (1982) as:

$$kB_s^{-1} = 2.46(\mathrm{Re}_*)^{0.25} - \ln(7.4) \qquad \text{(eq. 2.18)}$$

The within canopy wind speed profile extinction coefficient, n, is formulated as a function of the cumulative leaf drag area at the canopy top as:

$$n = C_d \cdot \frac{LAI}{2\frac{u_*^2}{u(h)^2}} \qquad \text{(eq. 2.19)}$$

where the leaf area index (LAI) is defined as:

$$LAI = NDVI \cdot \frac{1 + NDVI}{1.000001 - NDVI^{0.5}} \qquad \text{(eq. 2.20)}$$

and the normalized difference vegetation index (NDVI) derived from AVHRR band 1 & 2 surface reflectance is:

$$NDVI = \frac{r_2 - r_1}{r_2 + r_1} \qquad \text{(eq 2.21)}$$

2.3. Partial conclusion

In this chapter, we approached the general concepts, in the form of mathematical formulas, which constitute the base of the theory of SEBS. In the next one, the above-mentioned formulas will be re-examined in detail and they will be elucidated as they will be used as principal tool in this thesis.

CHAPTER 3: METHODOLOGICAL APPROACH: DATA ACQUISITION, DATA PROCESSING AND ACTUAL COMPUTATION

The advanced algorithms for the estimation of heat fluxes developed in the recent years by Alterra Green World Research have led to the computational scheme of the SEBS. As input data, SEBS needs satellite images in the visible, near infrared and thermal infrared frequency ranges and a data set of meteorological stations. The computational scheme ranges from acquisition and preprocessing of both meteorological and satellite data to estimate land optical parameters (albedo, soil temperature, emissivity, NDVI and fractional vegetation coverage), to the determination of roughness for heat transfer, friction velocity, sensible heat through models, and ends up with the determination of the evaporation fraction. To deal with the whole and complex calculations, on a pixel basis, that lead to each component of the SEBS (SEBS GUI V3.3), the version 3.6 of Environment for Visualizing Image, Research Systems Inc. (ENVI) package is used with its programming language Interactive Development Language, Research System, Inc. (IDL) on a Windows NT-2000 platform.

This chapter tends to enlighten all the five steps of the computational scheme in SEBS, shown in the flowchart of Figure 3.1. Summarily presented, the computational framework starts with getting usable data from the source data and data preprocessing as step 0 and step 1, respectively. The derivation of the land surface parameters follows as step 2 that leads to run SEBS in step 3. The end step (step 4) is to validate the SEBS output and check whether the study objectives are satisfied. While starting with the data description, let us approach the step 0 of the scheme: the input data collection.

3.1. Data retrieval

3.1.1 Satellite data ordering procedure

The NOAA satellite active archive (SAA) website provides a means to get remotely sensed data that are suitable for this study. In fact, from the web link www.saa.noaa.gov, one can register to access data by providing an email address, defining user preferences and choosing a password. By selection of Advanced Very High Resolution Radiometer (AVHRR) as a product type, you are directed to the page where criteria such as “data type”, “temporal and spatial coverage” have to be filled in. After that, you click on “search” and the result is displayed as a new page in the form of a table with columns consisting of e.g. “view details”, “shopping cart”, “inventory ID”, “data type name”,

“orbit”, “start time”, “end time”, “sat ID”, and “data set name”, that give characteristics and descriptions of each raw image. Each display page contains 10 raw images and by using the next or previous button one can navigate to the desired date-image. By clicking on “view details” for one raw image, one can have a quick look at both the satellite overpass time and the data (a panchromatic reduced image) one will get when they will become available. “Shopping cart” option is in form of a check box, on which you click to select a candidate image for ordering. Once a set of desired raw images is selected, the “Goto cart” option brings you to an overview of your selection, displays its size and presents the option to place the order if you are satisfied with the selection. When the order is placed, you will get an order number (a 7 digits like A1234567) and, in your mailbox, you will get a message announcing the reception and proceeding of the order. Within 24 hours you’ll be notified via your mailbox that all items of your order are available and you are requested to pick them up within 72 hours. In this message, an FTP file link is given which helps you copying your images. These images are downloaded to an appropriate folder where you can view them and proceed further with image manipulation and analysis.

In this project, all ordered NOAA/AVHRR 1b images have the local area coverage (LAC) as data type of 1.1 km spatial resolution with the spatial coverage set to 40N 18W and 60N 15E to position the Netherlands (50.4N 3.0E and 53.5N 7.5E) in the center of the obtained image. To be appointed for ordering, the satellite overpass period must be during the daytime (i.e. sun shining period); since there is no response in visible wavelength during the night; and for our LAC and spatial coverage, this overpass time duration (difference between the start and end time of a raw image) is about 10 to 12 minutes. Obviously other satellite images, taken outside of the daytime period, have a shorter satellite overpass time duration and are thus discarded. At an earlier stage of data collection, we sought for days with an average cloud cover, set by KNMI, to be less than or equal to 2 octa’s for all the six main meteorological stations in the Netherlands. But since the days appointed by the KNMI to be less cloudy (average cloud cover ≤ 2) often show cloudy NOAA images or no images at all, an intensive image ordering was applied on each day of each month to get a cloud free image for the whole of the Netherlands. Thus, among the long list of potential usable images, a set of 145 images representing 15 years (from 1989 to 2003) at the rate of a single image per month was selected and used for further computation.

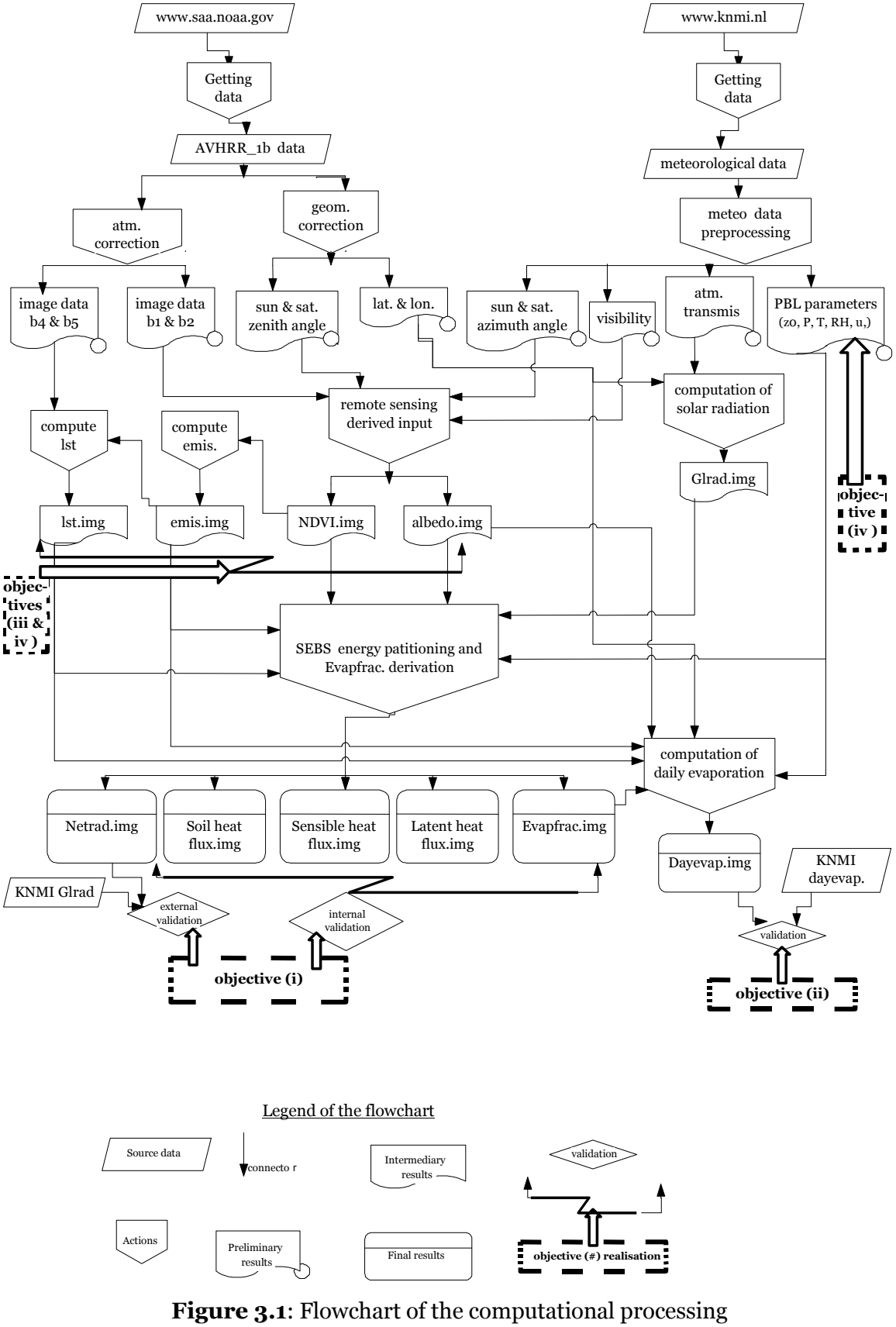

Figure 3.1: Flowchart of the computational processing

Dates, day number in a year, overpass times of the satellites along with the inventory ID (a unique code number of 7 digits identifying a satellite image in SAA archive) of our 12 used images of the year 2003 are listed in table 3.1 as an example, while the whole list of 180 used images together with other candidate images is presented in appendix 1 wherein the first twelve are the ones used in this thesis.

Table 3.1: Features of the 12 original NOAA/AVHRR images of 2003 used in the study

Date	Day number	Overpass time	Inventory ID
20031208	341	13.02	2941274
20031106	310	12.11	2914334
20031015	288	10.53	2889277
20030918	261	13.1	2856968
20030805	217	12.54	2820963
20030714	195	12.1	2809609
20030615	166	12.25	2795350
20030530	150	11.12	2787611
20030417	107	11.44	2766538
20030316	75	12.41	2750985
20030225	56	12.52	2741709
20030109	9	10.46	2685931

Source: NOAA data collection from www.saa.noaa.gov

One of the advantages of this intensive data ordering is that, from this study, a list or database (appendix 1) is obtained of less cloudy, LAC type NOAA/AVHRR1b images of the Netherlands potentially usable for other studies covering the period of 1989 to 2003 where for instance more than one image is needed per month. In that perspective, appendix 1 can serve as a lookup table to quickly select an image to be ordered from the SAA archive web page.

3.1.2. Meteorological data collection

For SEBS computation, the meteorological data needed are either ground surface values like surface air pressure, visibility, or computed atmospheric data at Planetary Boundary Layer (PBL) height. Meteorological stations directly measure the first while the latter are derived from these measured station data. That indicates the importance of field measurements as input data for SEBS. The Royal Dutch Meteorological Institute (KNMI) makes an on-line data time series of 6 main meteorological stations of the Netherlands (Den Helder, De Bilt, Groningen, Twenthe, Vlissingen and Maastricht) available via the link www.knmi.nl/product. From this website, archive data including the average

temperature, the minimum visibility, the air pressure and the mean wind speed have been downloaded for each of the 145 images used. For each of these four parameters and for each day, the arithmetic mean over the six stations was computed and retained as a value representing the entire country. Appendix 2 shows these values. Furthermore, use has been made of some of those parameters to derive the PBL parameter values needed. The data computation section will show step by step each process of PBL parameters derivation.

3.2. SEBS computation process

Many variables involved in SEBS computation are physical parameters to be derived by mathematical models. Others are empirical constants. In this section, we first show the table of all these empirical constants (Table 3.2) from literature and afterwards we illustrate the different formulas to derive the physical ones.

Table 3.2: SEBS input empirical constant-parameters

Parameters	Symbol (unit)	Default values used
Solar constant	I_{sc} (Wm^{-2})	1367
Air water vapor	W (g/cm^{-2})	1.92
Spectral emissivity difference of AVHRR bands 4 & 5	$\Delta\varepsilon$ (%)	0.002
Vegetation emissivity	ε_v (%)	0.98
Soil emissivity	ε_s (%)	0.95
PBL depth	z (m)	1000
Psychometric constant	γ (PaK^{-1})	67
Water vapor gas constant	R_v ($Jkg^{-1}K^{-1}$)	461.5
Dry air gas constant	R_d ($Jkg^{-1}K^{-1}$)	287.04
Latent heat of water vaporization	λ (Jkg^{-1})	$2.43.\ 10^{6}$
Gravitational acceleration	g ($ms^{-2)}$	9.8
Stefan-Bolzmann constant	σ ($Wm^{-2}K^{-4}$)	$5.678.\ 10^{-8}$
von Karman constant	k (-)	0.41

Source: Su *et al.* (2003a) p. 29

These constants are either used in the preprocessing computation (Excel calculation) explained hereafter or in the computation scheme through SEBS or in both.

3.2.1. PBL parameters computation from meteorological data

Some SEBS input parameters are obtained as a result of the preprocessing (Excel calculations) of the measured meteorological data. These parameters include:

- Air pressure at PBL-height

The PBL air pressure (i.e. air pressure at the reference height) is calculated using the measured air surface pressure P_a in the following formula:

$$P_{PBL} = P_a \left(\frac{44331 - ref.height}{44331 - alt} \right)^{\frac{1}{0.1903}} \qquad \text{(eq.3.1)}$$

where *alt* is the altitude of each station and the reference height is set to 1000 m. We opt for this formula instead of the conventional proposed P_{PBL} calculation formula that one can find in the literature due to the fact that the Netherlands is a flat country and the measured pressure is at the station height. Table 3.3 shows the altitude per station obtained from the KNMI (2nd column) and the factor of P_a (last column) to be used in (eq. 3.1).

Formula (eq. 3.1) is applied to each individual station in order to get the P_{PBL} per station. The mean over the six stations of each day is taken as the P_{BPL} value of the Netherlands to be used in the SEBS computation.

Table 3.3: Factor of P_a in (eq. 3.1)

Station	Alt (m)	(44331-1000)/(44331-alt)	[(44331-1000)/(44331-*alt*)]^(1/0.1903)
den Helder	0.5	0.9774534	0.8870667
de Bilt	2	0.9774865	0.8872245
Groningen	3.5	0.9775196	0.8873823
Twenthe	35.5	0.9782258	0.8907561
Vlissingen	8	0.9776188	0.8878558
Maastricht	114	0.9799625	0.8990976

Source: KNMI and self-computation

- Actual vapor pressure

Water in a gaseous state (i.e. water vapor) exerts a pressure just like other atmospheric gases. The partial pressure exerted by the water vapor present in a parcel is termed the "actual vapor pressure", symbolized by e and calculated according to the formula:

$$e = 622 \cdot \exp\left[\frac{17.67 \cdot T_a}{243.5 + T_a}\right] \qquad \text{(eq. 3.2)}$$

where T_a and e are the measured air temperature and pressure expressed in Celsius and Pascal, respectively [from http://members.aol.com/Accustiver/wxworld_calc.html].

- Saturation vapor pressure

The maximum partial pressure that water vapor molecules would exert if the air were saturated with water vapor at a given temperature is termed the saturation vapor pressure (e_s). It is directly proportional to the dew point temperature (T_d). Expressed in Pascal, we approach it with an empirical formula introduced by Bolton (1980) in http://hurri.kean.edu/~yoh/calculations/satvap/satvap.html, which yields only 0.3% error within the −35°C to 35°C temperature range:

$$e_s = 622 \cdot \exp\left[\frac{17.67 \cdot T_d}{243 \cdot 5 + T_d}\right] \qquad \text{(eq. 3.3)}$$

- PBL relative humidity

The relative humidity (RH) is the amount of water actually in the air divided by the amount of water the air can hold. RH is expressed as a percentage and can be computed in a variety of ways. For this research, we divided the actual vapor pressure (e) by the saturation vapor pressure (e_s) and then multiplied this by 100 to convert it to a percentage.

$$RH = \frac{e}{e_s} \cdot 100 \qquad \text{(eq. 3.4)}$$

Although there is more moisture (more water vapor) in the air in summer than in winter, one can notice that in winter e and e_s are close together and RH is high while the reverse situation is observed in summer where e and e_s are far apart and RH is low (see Table 3.4).

- PBL specific humidity

The mass of water vapor over an area divided by the total mass of the air over that area (including water vapor) is termed the specific humidity (q). It depends on the actual vapor pressure and total air pressure. At the PBL, it is approached with the formula (http://hurri.kean.edu/~yoh/calculations/moisture/Equations/moist.html):

$$q = \frac{622 \cdot e}{P_{PBL} - e} \qquad \text{(eq. 3. 5)}$$

where e is the actual vapor pressure and P_{PBL} the air pressure at the PBL, both expressed in Pascal and q in kg/kg.

- Potential temperature at PBL

The potential temperature (θ_a 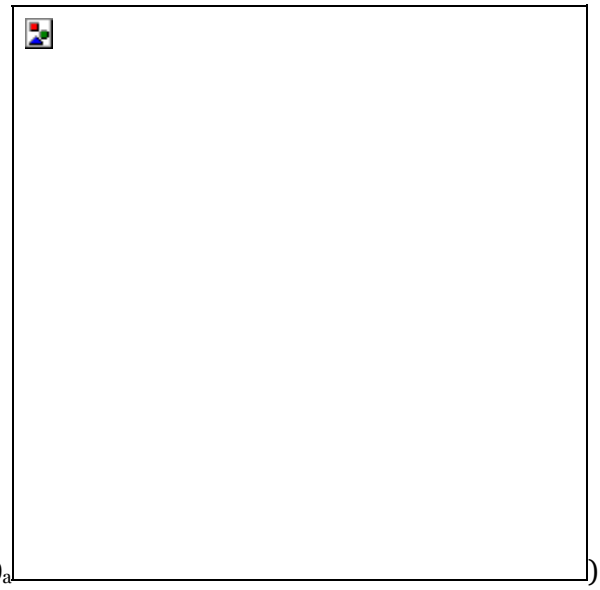) is defined as the temperature air would get if brought dry adiabatically (i.e. without exchange of energy with its environment) to 1000 mb. It allows one to determine the amount of internal energy air has (from http://www.srh.noaa.gov/ffc/html/gloss1.shtml). At the PBL, it depends on the actual surface temperature and the PBL pressure according to Poisson's equation as follows:

$$\theta_{PBL} = T_a \left(\frac{1000mb}{P_{PBL}} \right)^{0.286} \qquad \text{(eq 3.6)}$$

(from http://hurri.kean.edu/~yoh/calculations/diagnostic/diagnostic.html)

- Virtual potential temperature at PBL

The virtual potential temperature is the temperature a mass of air at a specific pressure level and virtual temperature would have if it were lowered or raised to 1000 mb. This is defined by Poisson's equation and in this project it is approached by the following formula:

$$\theta_v = T_a\left(1 + 0.61 \cdot q\right) \cdot \left(\frac{P_{PBL}}{P_a}\right)^{-0.286} \qquad \text{(eq. 3. 7)}$$

Table 3.4 illustrates the values of those parameters as a summary of preprocessing for the used dates in the year 2003.

Table 3.4: Measured and preprocessed input SEBS meteorological data for the year 2003

yyyymmdd	**Ta**	**Pa**	**P_{PBL}**	**e**	**e_s**	**RH**	**q**	**θ_a**	**θ_v**	**visibility**	**u**
	(^{o}C)	(pa)	(pa)	(pa)	(pa)	(%)	(kg/kg)	(^{o}C)	(^{o}C)	(km)	(m/s)
20031208	4.37	102622	91323	712	849	84	0.49	4.51	5.85	10.67	2.75
20031106	7.83	103042	91696	790	1079	73	0.54	8.10	10.76	5.68	2.80
20031015	10.30	102698	91391	849	1274	67	0.58	10.65	14.42	8.50	4.83
20030918	14.18	101720	90521	949	1645	58	0.65	14.66	20.52	3.53	3.85
20030805	17.87	102490	91205	1051	2081	50	0.72	18.47	26.58	9.08	3.72
20030714	16.87	101645	90453	1022	1954	52	0.71	17.44	24.95	14.70	4.50
20030615	14.62	102072	90833	960	1692	57	0.66	15.11	21.20	6.83	2.42
20030530	13.20	101487	90312	923	1543	60	0.64	13.65	18.96	6.55	2.98
20030417	7.73	102995	91655	788	1072	74	0.54	8.00	10.61	10.67	5.32
20030316	5.52	104222	92746	737	920	80	0.50	5.70	7.43	2.27	2.37
20030225	3.33	102145	90898	690	790	87	0.47	3.45	4.44	3.95	3.65
20030109	2.57	101995	90765	674	748	90	0.46	2.65	3.40	10.83	3.63

3.2.2. Land surface parameters from satellite data

Land surface parameters were derived from NOAA images. Their computation is incorporated in the SEBS process via the IDL event.pro file wherein all the formulas are explicitly presented and the output is an image file of each parameter per input day-image. Those parameters include:

- Albedo

According to Valiente *et al.* (1995) quoted by Su (2001), the surface albedo is obtained from the reflectance in bands 1 and 2 of the AVHRR 1b image by the following relation:

$$\alpha = 0.545 \cdot r_1 + 0.320 \cdot r_2 + 0.035 \qquad \text{(eq. 3.8)}$$

- NDVI

The following relation derives the normalized difference vegetation index from the reflectance of bands 1 and 2:

$$NDVI = \frac{r_2 - r_1}{r_2 + r_1} \qquad \text{(eq. 3.9)}$$

- Land surface emissivity

Caselles and Sobrino (1989) gave:

$$\varepsilon = \varepsilon_v f_c + \varepsilon_g (1 - f_c) + 4 \cdot < d\varepsilon > \cdot f_c \cdot (1 - f_c) \qquad \text{(eq. 3.10)}$$

where $f_c = \frac{NDVI - NDVI_{\min}}{NDVI_{\max} - NDVI_{\min}}$ is the vegetation fractional coverage and <dε> is a non-linear parameter set to 0.002; ε_v and ε_g are the emissivity for vegetation and soil, respectively, in the 10.5 – 12.5 μm spectral range and set to ε_v = 0.985 ±0.007 and ε_g = 0.960±0.010.

- Surface temperature

Coll and Caselles (1997) used the brightness temperature in bands 4 and 5 of AVHRR to compute the surface temperature according to the following formula:

$$T_0 = T_4 + \left[1.34 + 0.39(T_4 - T_5)^2 + 0.56 + \chi(1 - \varepsilon) - \beta \cdot \Delta\varepsilon\right] \qquad \text{(eq. 3.11)}$$

with ε the mean surface emissivity of bands 4 & 5; Δε the spectral emissivity difference of bands 4 & 5; $\beta = 150\left(1 - \frac{W}{4.5}\right)$; $\chi = W^3 - 8W^2 + 17W + 40$ and W the atmospheric water vapor content.

3.2.3. Method to derive roughness lengths for momentum and heat transfer

Parameterization models for estimation of the roughness lengths for momentum and heat transfer have been developed based on remote sensing data. Su *et al.* (2003a) proposed the following relationship between the momentum transfer roughness length and the vegetation index and this is used in this thesis:

$$z_{0m} = 0.005 + 0.5 \cdot \left(\frac{NDVI}{NDVI_{\max}}\right)^{2.5} \qquad \text{(eq.3. 12)}$$

The zero-plan displacement height d is expressed as: $d = 4.9 \times z_{om}$

Using the set of equations (eq. 2.16) and (eq. 2.17) one can determine the heat transfer roughness length, z_{oh}. Table 3.5 (below) shows the summary of these parameterization schemes.

Table 3.5: SEBS input variables and their source

Parameters or variables	**Symbol (unit)**	**Source or parameterization**
Albedo	α (-)	AVHRR data bands 1& 2
Normalized Difference Vegetation Index	NDVI (-)	AVHRR data bands 1& 2
Emissivity	ε (-)	NDVI
Atmospheric emissivity	ε'(-)	$9.26 \times 10^{-6} \times T_a^2$
Vegetation fractional coverage	f_c (-)	NDVI
Leaf area index	LAI (-)	NDVI
Displacement height	d (m)	$z_{om} \times 4.9$
Roughness length for momentum transfer	z_{om} (m)	NDVI
Roughness length for heat transfer	z_{oh} (m)	Model computation
Wind speed at the top of canopy	u(h) (ms^{-1})	u, d, z_{om}

Land surface temperature	T_o (K)	AVHRR data bands 4& 5
Saturation vapor pressure	e_s (pa)	T_o, T_a
Actual vapor pressure	e (pa)	Land surface air temperature, dew-point air temperature, P_a
Solar radiation	R_{sw} (Wm^{-2})	Year, month, date and time with τ (-)

Source: Su *et al.* (2003a)

3.2.4. Geometric correction

ENVI built-in functionalities offer the possibility to easily geometrically correct an AVHRR 1b image and make it ready-to-use (suitable) for this study. Two steps were necessary for this purpose.

The first step was the radiometric calibration where the digital numbers of the original AVHRR 1b image were converted to reflectance and radiance (brightness) values. Thus, bands 1 and 2 were calibrated to percent reflectance and bands 3, 4 and 5 to brightness temperature in Kelvin. The outcome-calibrated image was then geo-referenced, subset to fit only the Netherlands (study area), and split into 4 files representing percent reflectance of band 1, and band 2, and temperature (K) of band 4 and band 5. Band 3 was discarded since it is not needed for further calculation in SEBS.

The second step was to derive the geometry file of latitude, longitude, solar and sensor zenith angles, which in turn was also geo-referenced, subset, and split into 4 files representing each of these geometrical elements.

For purpose of geo-referencing within this project, the Universal Transverse Mercator (UTM) projection, zone 31 North and datum of WGS-84 were used. For image registration, the triangulations warp points and the nearest neighbor resampling methods with 51 warp points on the x-axis and 150 warp points on the y-axis were applied.

For fitting the study area of the whole Netherlands, the subset criteria were set to the map coordinates in meters as: upper left coordinates (519910.59E; 5939697.31N) and lower right coordinates (788310.59E; 5623997.31N). This represents an image size of 246 samples (or columns) for 289 lines with a pixel size of 1100 m.

From the http://edcdaac.usgs.gov/gtopo30/hydro/europe.html website, the European digital elevation model (DEM), slope, and aspect were downloaded, converted and a subset taken for the Netherlands. UTM projection zone 31 North and a spatial resolution

of 1.1 km were chosen to fit the characteristics of the input NOAA/AVHRR 1b data. The three data (DEM, aspect and slope) were combined with latitude and longitude geometry files of each NOAA image to obtain the solar zenith and azimuth angles along with sensor zenith and azimuth angles, needed in SEBS computation.

3.2.5. Global radiation

The incoming global radiation was calculated for each image on a pixel basis, according to the following equations:

$$K^{\downarrow} = e_0 I_{sc} \cos(SZA).\tau_a \qquad \text{(eq. 3.13)}$$

with SZA as the solar zenith angle derived for each pixel, e_o the eccentricity-orbiting correction factor

$$e_0 = 1.00011 + 0.034221\cos(da) + 0.00128\sin(da) + 0.000719\cos(2.da) + 0.000077\sin(2.da) \qquad \text{(eq. 3.14)}$$

da, the date angle; is given by:

$$da = 2\pi.(D_{day} - 1)/365 \qquad \text{(eq. 3.15)}$$

with D_{day} accounting for Julian day number, ranging from D_{day} =1 for January the 1st until D_{day} = 365 for December the 31st . For the year 2003, table 3.6 shows the dates, D_{day}, da and e_o for the image recordings.

Table3.6: Input values for global radiation calculation

yyyymmdd	Dday	da	e_o
20031208	342	5.87	1.03
20031106	310	5.32	1.02
20031015	288	4.94	1.01
20030918	261	4.48	0.99
20030805	217	3.72	0.97
20030714	195	3.34	0.97
20030615	166	2.84	0.97
20030530	150	2.56	0.97
20030417	107	1.82	0.99
20030316	75	1.27	1.01

20030225	56	0.95	1.02
20030109	9	0.14	1.03

3.2.6. Daily evaporation derived from SEBS

When the evaporative fraction is known, the daily evaporation is determined as follows:

$$E_{daily} = 8.64 \cdot 10^7 \cdot \overset{24}{\underset{0}{\Lambda}} \cdot \frac{R_n - G_0}{\lambda \rho_w} \qquad \text{(eq. 3.16)}$$

where E_{daily} is the actual evaporation on a daily basis, expressed in mmd^{-1}. $\overset{24}{\underset{0}{\Lambda}}$ is the daily evaporative fraction, which can be approximated by the SEBS estimate since the evaporative fraction is conservative during a day (24 hours). R_n and G_o are the daily net radiation flux and soil heat flux, respectively; λ is the latent heat of vaporization expressed in Jkg^{-1}; ρ_w is the density of water in kgm^{-3}.

The latent heat flux of vaporization is calculated as:

$$\lambda = \left[2.501 - 0.00237 \cdot T_{air}\right] \cdot 10^6 \qquad \text{(eq. 3.17)}$$

with T_{air} the mean air temperature in Celsius. Because the downward flux in daytime and the upward flux at night balance each other approximately, the daily soil heat flux is close to zero and the evaporation depends only on the net radiation flux. Thus (eq. 3.16) can be rewritten as follows:

$$E_{daily} = 8.64 \cdot 10^7 \cdot \overset{24}{\underset{0}{\Lambda}} \cdot \frac{R_n}{\lambda \rho_w} \qquad \text{(eq. 3.18)}$$

The daily net radiation is given by:

$$R_n = (1 - \alpha) \cdot K_{24}^{\downarrow} + L_{24} \qquad \text{(eq. 3.19)}$$

in which L_{24} is the daily net long wave radiation and $K_{24}^{\downarrow}$ is the daily incoming global radiation. $K_{24}^{\downarrow}$ is a function of the atmospheric transmittance (τ_a); the earth-sun distance (D); the latitude of the observation site (*alt*), the solar hour angle (ω); and the solar declination (δ), according to the following formulas:

$$K_{24}^{\downarrow} = 435.2\tau_a \cdot D \cdot \left(\omega \sin(lat)\sin(\delta) + \cos(lat)\cos(\delta)\sin(\omega)\right) \quad \text{(eq. 3.20)}$$

in which

$$\delta = 0.409\sin(0.0172D_{day} - 1.39) \quad \text{(eq. 3.21)}$$

$$D = 1 + 0.33\cos(0.0172D_{day}) \quad \text{(eq. 3.22)}$$

$$\cos(\omega) = -\tan(lat)\cdot\tan(\delta) \quad \text{(eq. 3.23)}$$

D_{day} represents the Julian day number.

The daily net long wave radiation L_{24} depends on the air and surface temperatures, T_a and T_o, according to the formula:

$$L_{24} = \varepsilon_a \sigma T_{air}^4 - \varepsilon\sigma T_0^4 \quad \text{(eq. 3.24)}$$

σ is the Stefan-Boltzmann constant; ε_a is the emissivity of the clear sky which is estimated by Swinbank (1963) quoted by Su (2001a) as follows:

$$\varepsilon_a = 9.2\cdot 10^{-6}\cdot\left(\overline{T_a} + 273.15\right)^2 \quad \text{(eq. 3.25)}$$

where $\overline{T_a}$ is the daily average air temperature.

3.3. Partial conclusion

To end this chapter, we can state that it involves and treats the most important concepts regarding SEBS input parameters and its theory. One should bear in mind that, although we approach these concepts with a lot of formulas, it is not necessary to be expert in mathematics before using SEBS. Of course it is worthwhile to understand what you are doing and be able to find out errors. At all time, earth sciences in general and hydrometeorology science in particular involve a lot of mathematics. Some simplifications and assumptions were made during this presentation that is why, for instance, we didn't elaborate on the stability correction function. We chose a fixed value for the reference height just to mention a few. The interested reader may refer to appropriate cited literatures.

While the corrected input data are filled in the SEBS scheme, the process outputs are a number of image files. Showing the results of SEBS processing and its validation with KNMI measurements is the subject of the next chapter.

CHAPTER 4: RESULTS, ANALYSIS, VALIDATION AND DISCUSSION

Introduction

The general results of the computations and processing are presented and discussed hereafter. First of all, the input remote sensing image-derived data such as albedo, land surface temperature and normalized difference vegetation index are presented in that sequence. Then follow the results of the SEBS derived energy partitioning and evapotranspiration on the earth surface. Since we are focusing on the climatological aspects of our processing results, we discuss the mean over the 15 years study period rather than the individual monthly or yearly results. Successively are presented the map of July 14th 2003 for illustration purpose, the graph of mean values and that of range values (minimum, maximum and mean) over the 15 years for the parameters generated by SEBS computations. Our expectation in using SEBS for this long-term study is that each of the derived parameters has, more or less, a similar distribution within a year, i.e. values increase gradually from January to June/July and decrease from there to December. Moreover, we expect a low monthly variability from one year to another throughout the period of the study since KNMI did not record an extremely dry or very wet year in that period. In that respect, we capture the important features of the aforementioned graphs by a few summary statistics. These statistics include the measure of location to get an idea of where the center of the distribution lies, the measure of spread to describe the variability of the data and the measure of shape to provide information on the symmetry and the length of the tail for data distribution. Then we use, respectively, the mean, the standard deviation (st.dev) and the coefficient of variation (CV). Here, an absolute value of CV greater than one ($|CV|>1$) can provide some warning of the presence of some erratic high or low values that may have significant impact on the final result (Isaaks and Srivastava, 1989). The general tables, showing the values per month within each year of the study period (data organization), can be found in the appendix 3, 4 and 5a. Comparing our output results with values measured by the Royal Netherlands Meteorological Institute (KNMI) is done for final validation. Appendix 5b shows the graphs of the daily evaporation validated against KNMI measurements.

4.1 Input remote sensing derived data

4.1.1. Albedo

Plate 1a shows the map of albedo over the Netherlands as derived by remote sensing processing for July 14th 2003. This map outlines the general pattern of surface albedo and its conformity as one can expect in July for the Netherlands. Water surface values range from 3% to 6%; the most part of the land surface values range from 10% to 20% with the highest values found in the northern part of the country that go up to 25% and cover only a few pixels of the image.

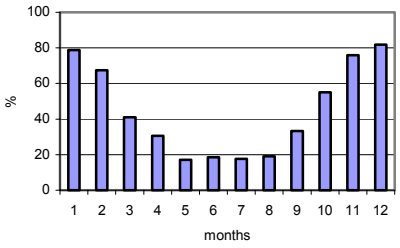

Figure 4 1a: Graph of mean Albedo values over 15 years

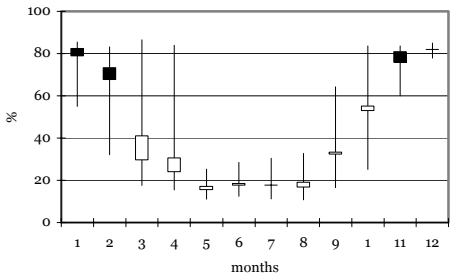

Figure 4.1b: Albedo range values over 15 years

Table4.1: Summary statistics of monthly albedo values (in %) over 15 years.

month	Measure of						
	location				spread	shape	
	max	min	mean	median	st.dev	CV	skew
Jan	85.49	55.00	78.81	82.48	9.49	0.12	-2.40
Feb	83.20	32.06	67.52	73.38	16	0.24	-1.35
Mar	86.54	17.51	41.04	29.52	24.9	0.61	0.97
Apr	83.94	15.43	30.55	23.89	18.9	0.62	2.00
May	25.30	11.13	17.15	15.41	4.76	0.28	0.69
Jun	28.52	12.38	18.47	17.56	5.5	0.3	0.59
Jul	30.47	11.16	17.59	17.73	5.51	0.31	1.03
Aug	32.69	10.78	19.04	16.63	5.89	0.31	1.21
Sep	64.18	16.49	33.33	32.26	12.6	0.38	1.22
Oct	83.71	25.12	55.10	52.89	20.3	0.37	0.19
Nov	83.58	59.95	75.81	80.89	9.42	0.12	-1.128
Dec	85.05	77.91	81.81	81.98	1.96	0.02	-0.45

The long-term averaged values of the albedo per month over a period of 15 years are illustrated by the graph that is shown in Figure 4. 1a. That graph of the monthly average trend over the 15 years study period tells a little bit about the variability from one month to another during that period. Figure 4.1b illustrates that a big variability is observed in

February, March, April, September and October where the range can span from 15% (min) to 85% (max). Table 4.1 shows the summary statistics of albedo values for the 15 years study period per month. Valuable information contained in the graph of Figure 4.1b is explained in the summary statistics table (Table 4.1). The fact that all the coefficients of variation (CV) values are lower than one shows the lack of high erratic values. A long tail of low albedo values (skew <0) characterized the winter period (November to February) and the growing season was characterized by the long tail of high albedo values (skew >0) with remarkably high values in April, July, August and September. The non-zero skewness coefficients (skew) indicate that none of the monthly albedo values distribution is normal, but the asymmetry is not too skewed, which is confirmed by the closeness values of mean and median. Thus potentially, the use of albedo may not cause big errors in evapotranspiration estimation by SEBS. Cloud and/or snow effects on the used satellite images explain the high albedo values found in winter (where max≥83%).

4.1.2. Land surface temperature (lst)

Plate 1b shows the map of land surface temperature (lst) over the Netherlands as derived from remote sensing processing for July 14th 2003. This map outlines the general pattern of land surface temperature for the Netherlands on that day and values range from 19°C to 38°C. Water surface values range from 18 to 21°C; the most part of the land surface values are ranged from 21 to 31°C with hot spot values (31-37°C) found in the center and southern parts of the country over only few pixels of the image.

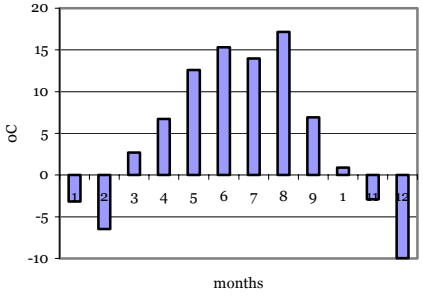

Figure 4.2a: Graph of mean SEBS_lst values over 15 years

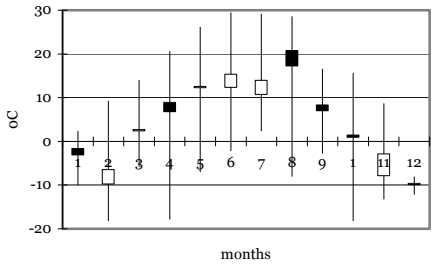

Figure 4.2b: SEBS_lst range values over 15 years

The monthly averaged values of the land surface temperature over the study period of 15 years are illustrated by the graph of Figure 4.2a. From that graph, it is clear that surface temperature is always below zero in the winter period (November to February) and above zero during the growing season (March to October). The monthly variability of the land surface temperature from one year to another of the study period is illustrated by Figure 4.2b along with the table of the summary statistics (Table 4.2). Neither the figure nor the table helps to clearly define and understand the parameter's distribution. Only one can remark some erratic values from October to April where the absolute value of CV is greater than one. Also the growing season (March to October) shows a long tail of low surface temperature values (skew<0) with a big variability (T_{max} minus T_{min}) ranging from 19°C in March to 38°C in April. One can expect this factor to introduce some systematic errors in our daily evaporation estimation afterwards.

Table4.2: Summary statistics of monthly Sebs_lst values over 15 years

month	Measure of						
	location				spread	shape	
	max	min	mean	median	st.dev	CV	skew
Jan	2.33	-9.98	-3.15	-1.63	5.44	-1.73	-0.45
Feb	9.22	-18.15	-6.46	-9.79	9.00	-1.39	0.66
Mar	13.94	-5.78	2.71	2.31	7.00	2.58	0.27
Apr	20.57	-17.82	6.71	8.94	11.32	1.69	-0.78
May	26.12	-6.94	12.61	12.20	8.65	0.69	-0.46
Jun	29.45	-2.12	15.32	12.28	9.90	0.65	-0.20
Jul	29.10	2.42	13.96	10.67	9.82	0.70	0.33
Aug	28.57	-7.97	17.17	20.76	11.08	0.65	-1.23
Sep	16.52	-2.74	6.92	8.35	5.69	0.82	-0.21
Oct	15.59	-18.18	0.89	1.45	9.57	10.76	-0.51
Nov	8.60	-13.22	-2.89	-7.90	10.11	-3.50	0.44
Dec	-8.14	-12.10	-9.95	-9.61	2.00	-0.20	-0.74

4.1.3. Normalized difference vegetation index (NDVI)

In Plate 1c, the map of the normalized difference vegetation index (NDVI) of July 14th 2003 is presented wherein values are ranged from 19% to 77%. The NDVI of a water body is set to zero value. Most of the land pixels have a value between 28% to 77% with spots of lowest values from 19% to 27% found in the provinces of Noord Holland and the north of Zuid Holland over few image pixels. This map matches the expectation for the

Netherlands in July where we have full green vegetation coverage with high values of NDVI.

The graph of the monthly NDVI values averaged over 15 years in Figure 4.3a shows a shape of quite a normal distribution. Figure 4.3b illustrates the NDVI values' variability within each month. The growing season (March to October) except July shows a tail of low NDVI values along with a big difference between the minimum and maximum values.

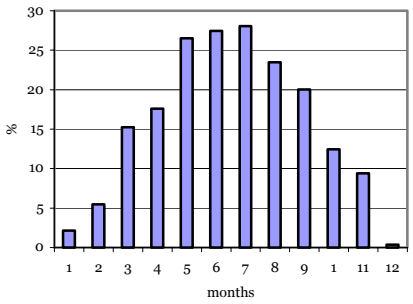

Figure 4.3a: Graph of mean NDVI values over 15 years

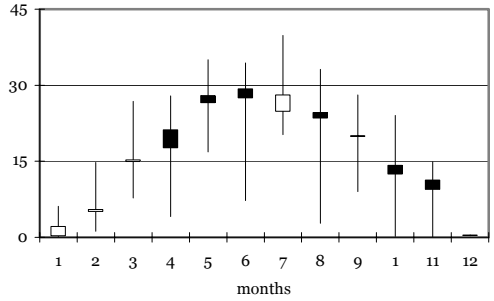

Figure 4.3b: NDVI range values over 15 years

Table4.3: Summary statistics of monthly NDVI values over 15 years

month	Measure of location				spread	shape	
	max	min	mean	median	st.dev	CV	skew
Jan	6.10	0.16	2.14	0.28	2.71	1.27	0.98
Feb	14.77	1.18	5.47	5.06	4.66	0.85	1.52
Mar	26.80	7.78	15.25	14.90	5.16	0.34	0.72
Apr	27.90	4.10	17.59	21.22	7.09	0.40	-0.45
May	35.01	16.83	26.53	27.99	5.70	0.21	-0.33
Jun	34.38	7.25	27.44	29.30	7.27	0.26	-2.00
Jul	39.85	20.24	28.06	24.78	6.29	0.22	0.62
Aug	33.14	2.78	23.46	24.63	7.76	0.33	-1.42
Sep	28.11	9.04	20.02	19.88	5.74	0.29	-0.24
Oct	24.04	0.16	12.45	14.20	7.69	0.62	-0.53
Nov	14.89	0.13	9.41	11.31	6.73	0.71	-1.20
Dec	0.43	0.29	0.36	0.36	0.10	0.27	-

That is confirmed again in the table of the summary statistics (Table 4.3) with negative values of skewness coefficients (skew<0). Erratic values are found in January (CV>1), a tail of high NDVI values in February (skew>0) and a tail of low ones in November (skew<0) are the main characteristics of NDVI values no-trend in wintertime where there is almost no vegetation except some sparse coniferous species along with snow and cloud effects. One can expect NDVI to introduce, at a certain extent, some systematic

errors in our daily evaporation estimation regardless its normal distribution, especially because this factor is used as input data on several occasions in the SEBS process.

4.2. SEBS derived energy partitioning

4.2.1. Net radiation (R_n)

The available solar energy at the earth surface is termed the net radiation (R_n). That indicates the energy that is considered as input for the evapotranspiration process (sensible and latent heat fluxes) and ground heat flux as well as for photosynthesis reactions of the green vegetation. Plate 2a illustrates the map of the instantaneous pattern over the Netherlands of that energy during the satellite overpass time on July 14th 2003. For this instantaneous pattern, the whole country of the Netherlands land surface value is ranged from 311 to 440 W/m². The water bodies close to the land (inter-land water body like: IJselmeer, Waddenzee, Haringvliet, Westerschelde and Oosterschelde) and some spots inside the land have a value of 440 to 570 W/m² and the highest values of the net radiation are found in the Noordzee water body.

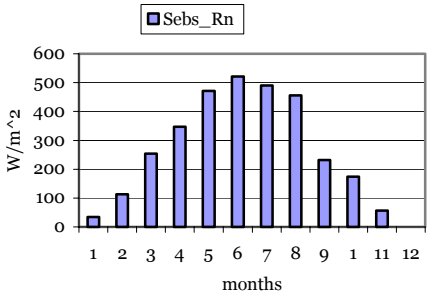

Figure 4.4a: Graph of mean R_n values over 15 years

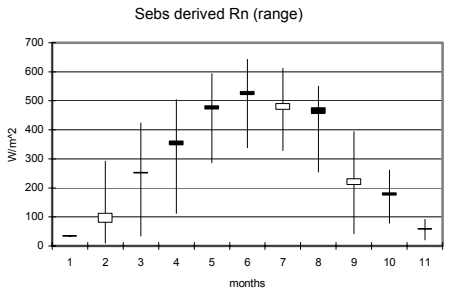

Figure 4.4b: SEBS_R_n range values over 15 years

Table4.4: Summary statistics of monthly R_n values over 15 years.

month	Measure of location				spread	shape	
	max	min	mean	median	st.dev	CV	skew
Jan	34.14	34.14	34.14	34.14	-	-	-
Feb	291.87	9.77	112.9	80.37	108.1	0.958	1.01
Mar	423.37	33.76	254	249.8	119	0.468	-0.4
Apr	503.54	112.9	346.9	362	124.2	0.358	-0.6
May	593.36	287.04	471	483.1	97.95	0.208	-0.6
Jun	642.55	338.85	520.7	532.1	76.75	0.147	-0.9
Jul	612.2	328.41	490.6	469.1	89.97	0.183	-0.2
Aug	550.2	254.29	456.3	475.7	79.53	0.174	-1.4
Sep	394	41.41	231.9	210.6	112.5	0.485	0
Oct	260.9	78.19	173.8	182.8	71.12	0.409	-0.2

Nov	91.12	20.64	56.94	59.06	35.29	0.62	-0.3
Dec	-	-	-	-	-	-	-

The graph of the monthly net radiation values averaged over 15 years in Figure 4.4a shows quite a normal distribution shape. The SEBS derived net radiation's overall distribution for the Netherlands shows good results where experience from the past indicates that the maximum R_n value might not exceed 650 W/m². On behalf of its partitioning later, this is likely to be a good start for available energy in the evapotranspiration estimation process in SEBS. Figure 4.4b illustrates the monthly variability of the R_n values from one year to another of the study period. Large differences between minimum and maximum values of R_n are found from February to September. In the table of the summary statistics (Table 4.4), negative values of skewness coefficients indicate the presence of tails of low net radiation values during the study period particularly in the growing season (from March to October). That could be a big drawback while using low R_n values in the later stage of evapotranspiration estimation. Indeed, a lower available energy amount could reduce the amount dedicated for evaporation purpose and then lead to an under estimation of the evaporation.

4.2.2. Soil heat flux (G_o)

Plate 2b shows the map of the instantaneous distribution of the soil heat flux energy at the satellite overpass time of July 14th 2003. In this map, the land has values from 29 to 92 W/m². Few pixels with soil heat flux values up to 155 W/m² are found in the province of Noord Holland and Utrecht. The water surfaces have values ranging from 155 to 281 W/m². High values found in the water body can be explained mainly by the fact that the parameterization for G0 was only valid from bare soil to full vegetation and thus water was not treated separately. So, the use of the same G_o equation for water is questionable and even needs to be re-parameterized.

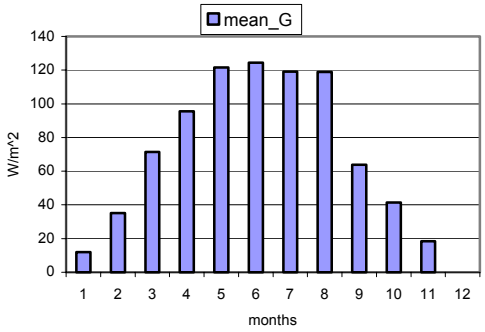

Figure 4.5a: Graph of mean G_o values over 15 years

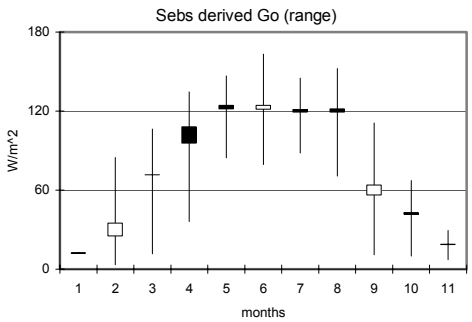

Figure 4.5b: SEBS_G_o range values over 15 years

During the growing season, for the Netherlands where De Bruin & Stricker (2000) found that G_o is often too small compared to R_n, the general expectation would be values around 35 W/m² (i.e. 5% of max R_n) when the net radiation is about at its maximum of 600 W/m² in the May-August period. Whether the SEBS method gives more weight to the ground heat flux should be looked into in the later stage of this study during the validation part. The graph of mean soil heat flux values over the study period (1989-2003) is shown in Figure 4.5a. That graph shows a normal shape that achieves its maximum around 120 W/m² in May-August. The summary statistics table (Table 4.5) illustrates an overall tail of low ground flux values (skew<0). This raises again the question to know if the SEBS algorithms do not give too much weight to this parameter. In fact, if the SEBS algorithm had given less weight to G0 then its average value in every image would be lower than what it is currently and therefore G0 would be in the expected range. The consequence of this is that one can expect that this high value of G0 does not allow having access to enough energy remaining for the evaporation process from which an underestimation is foreseen.

Table4.5: Summary statistics of monthly G_o values over 15 years.

month	**Measure of**						
	location				**spread**	**shape**	
	max	**min**	**mean**	**median**	**st.dev**	**CV**	**skew**
Jan	12.06	12.06	12.06	12.06	-	-	-
Feb	84.86	3.41	35.08	25.06	31.94	0.91	0.84
Mar	106.50	11.56	71.33	71.68	30.05	0.42	-0.77
Apr	134.54	36.12	95.48	108.08	30.99	0.32	-0.74
May	146.60	84.42	121.48	124.47	19.79	0.16	-0.58
Jun	163.15	79.38	124.33	121.30	21.10	0.17	-0.31
Jul	144.90	88.09	119.14	121.29	17.55	0.15	-0.37
Aug	152.33	70.76	118.92	121.67	21.46	0.18	-0.67
Sep	111.04	10.98	63.87	56.14	29.43	0.46	-0.05
Oct	67.23	9.87	41.45	42.98	19.90	0.48	-0.40
Nov	29.42	7.23	18.50	18.86	11.10	0.60	-0.14
Dec	-	-	-	-	-	-	-

4.2.3. Sensible heat flux (H)

Plate 2c shows the general pattern of the sensible heat flux on July 14th 2003 at 12.01 GMT (the satellite overpass time). In the map, most of the land surface values range from 232 to 348 W/m² and water body values are lower than 116 W/m². The highest values (348-465 W/m²) are found in the western and southern parts of the country.

The graph of the mean sensible heat flux values over 15 years is shown in Figure 4.6a and achieves its maximum (198 W/m²) in May. The distribution is not normal as there are no zero skewness coefficients. Figure 4.6b shows an overall tail of lower values of the sensible heat (skew<0) during the growing season and in February rather a tail of high values is obtained. Considering the fact that the sensible heat contributes a lot to evaporation estimation, the lower values are likely to lead to induce a great inaccuracy in evaporation estimation.

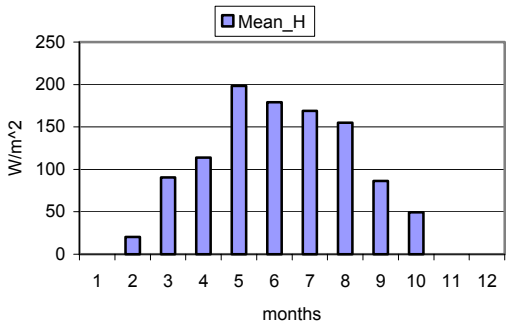

Figure 4.6a: Graph of mean H values over 15 years

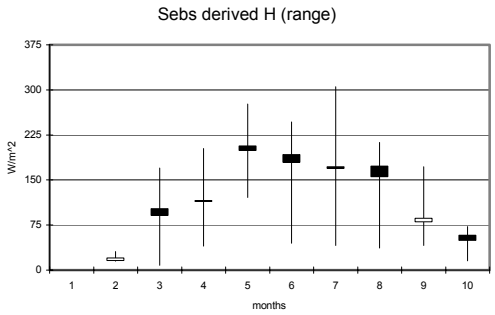

Figure 4.6b: SEBS_H range values over 15 years

All the trends described above are seen in the table of summary statistics (Table 4.6).

Table4.6: Summary statistics of monthly H values over 15 years.

month	Measure of location				spread	shape	
	max	min	mean	median	st.dev	CV	skew
Jan	-	-	-	-	-	-	-
Feb	30.99	15.03	20.48	15.43	9.10	0.44	1.73
Mar	169.70	8.13	90.65	102.05	56.24	0.62	-0.37
Apr	202.40	39.98	114.04	115.61	51.80	0.45	0.23
May	276.69	121.10	198.52	206.47	47.62	0.24	-0.30
Jun	246.60	44.67	179.05	192.15	53.77	0.30	-1.24
Jul	305.12	40.92	168.87	172.09	76.39	0.45	-0.08
Aug	212.67	36.72	155.15	173.25	54.97	0.35	-1.27
Sep	171.79	40.90	86.18	79.82	39.80	0.46	1.22
Oct	72.23	15.68	49.21	58.20	21.95	0.45	-0.96
Nov	-	-	-	-	-	-	-
Dec	-	-	-	-	-	-	-

4.2.4. Latent heat flux (λE)

The latent heat flux is often considered as the residual part of the energy balance at the earth surface. Plate 2d shows the general pattern of the latent heat flux of July 14th 2003. From that map, it can be said that the latent heat flux is scaled in an east-west gradient.

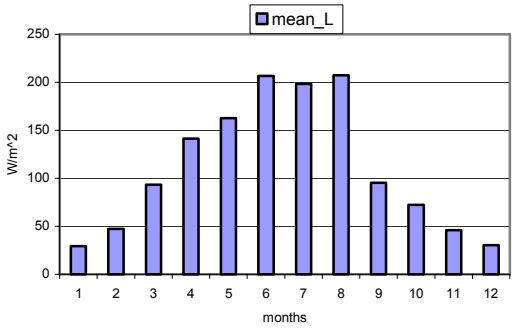

Figure 4.7a: Graph of mean λE values over 15 years

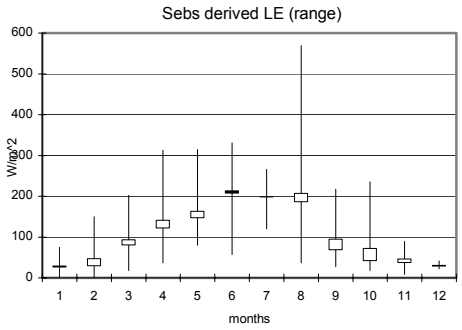

Figure 4.7b: SEBS_λE range values over 15 years

Table4.7: Summary statistics of monthly λE values over 15 years.

month	Measure of location				spread	shape	
	max	min	mean	median	st.dev	CV	skew
Jan	75.17	0.01	29.37	25.90	25.94	0.88	1.13
Feb	149.97	1.06	47.43	28.70	46.91	0.99	1.52
Mar	202.07	17.72	93.17	80.19	55.21	0.59	0.58
Apr	312.74	36.80	141.35	121.42	90.46	0.64	0.85
May	314.44	80.25	162.80	146.81	68.28	0.42	1.13
Jun	331.01	56.88	206.69	213.01	62.69	0.30	-0.57
Jul	266.16	119.67	198.34	197.53	41.72	0.21	-0.20
Aug	569.26	36.82	207.18	185.59	124.46	0.60	1.91
Sep	217.05	27.71	95.20	68.14	61.36	0.64	1.16
Oct	235.02	18.36	72.44	41.44	67.75	0.94	2.10
Nov	89.71	8.39	46.07	36.75	37.06	0.80	0.32
Dec	41.32	21.88	30.46	28.17	9.92	0.33	0.98

The western part of the Netherlands has a value range from 0 to 142 W/m² and the eastern part from 142-284 W/m². The inter land water body has a value from 284 to 426 W/m² while the Noordzee shows the highest values (up to 568 W/m²) of latent heat flux.

The graph of the mean latent heat flux values over 15 years is shown in Figure 4.7a. The maximum (206 W/m^2) is reached in June-August. The distribution is not normal. The variability of the latent heat flux value within each month from one year to another during the study period is illustrated in Figure 4.7b along with the table of summary statistics (Table 4.7). The biggest variability is observed in August. The graph and the table show an overall tail of high values except for June and July where there is a tail of low values. This fact could indicate that there is an overestimation of the latent heat flux and this may lead to less accurate values of evapotranspiration.

4.3. SEBS derived evapotranspiration

After deriving all these parameters in SEBS, one reaches now the state to use this information in the evaporation estimation. Hereafter, we present the output of the processing as evaporative fraction at the first stage. In case of a successful attempt, the evaporative fraction can lead to an estimation of the daily evaporation in combination with the net radiation and the water density constant when assuming that the soil heat flux increase during the day and decrease during the night are all in balance and also with the assumption that the evaporative fraction does not vary during the sunshine period of the day.

4.3.1 Evaporative fraction (EF)

The map of the evaporative fraction of July 14th 2003 is presented in Plate 3a. The general pattern of that map shows a gradient north south. In that respect, from the south to the center including the provinces of Gelderland and Utrecht and all the northwestern provinces of the Netherlands have evaporative fraction values ranging from 0 to 0.34. The northern and northeastern parts of the country have values ranging from 0.34 to 0.89 and the water body has a value from 0.89 to 1, i.e. potential evaporation.

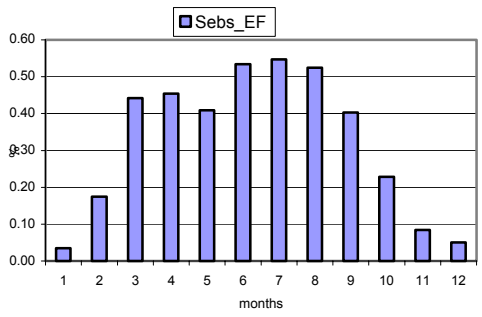

Figure 4.8a: Graph of mean EF values over 15 years

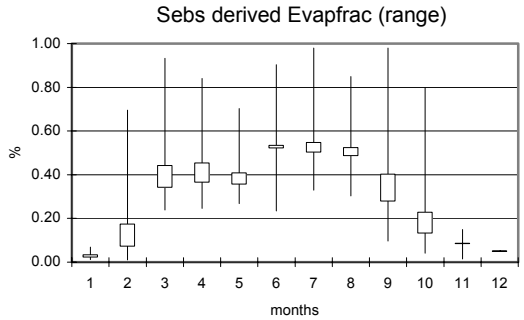

Figure 4.8b: SEBS_EF range values over 15 years

Figure 4.8a shows the graph of the monthly evaporative fraction values averaged over 15 years. The overall trend of that graph shows a normal distribution with the maximum around the June-August period. May shows rather low values that not match the general trend. The variability within each month during the study period is shown in Figure 4.8b along with the summary statistics table (Table 4.8).

Table4.8: Summary statistics of monthly EF values over 15 years.

month	**Measure of**						
		location			**spread**	**shape**	
	max	**min**	**mean**	**median**	**st.dev**	**CV**	**skew**
Jan	0.07	0.01	0.03	0.02	0.03	0.88	1.54
Feb	0.69	0.01	0.17	0.07	0.23	1.33	1.75
Mar	0.93	0.24	0.44	0.34	0.22	0.50	1.12
Apr	0.84	0.25	0.45	0.36	0.19	0.43	0.89
May	0.70	0.27	0.41	0.36	0.14	0.34	1.19
Jun	0.90	0.23	0.53	0.52	0.17	0.31	0.44
Jul	0.98	0.33	0.55	0.50	0.20	0.36	1.13
Aug	0.85	0.30	0.52	0.49	0.15	0.28	0.88
Sep	0.98	0.10	0.40	0.28	0.26	0.64	1.21
Oct	0.80	0.04	0.23	0.13	0.25	1.09	2.08
Nov	0.15	0.02	0.08	0.09	0.07	0.80	-0.18
Dec	0.05	0.05	0.05	0.05	-	-	-

In wintertime one can see erratic high values of evaporative fraction outlined by a CV value close to 1 or bigger. All the months show a tail of high values with skew>0 especially in the growing season where skew>1. According to expectation for the Netherlands, the values for EF are in general low, especially during the growing season (0.23<EF<0.55) period, during which the evaporative fraction rarely falls below 0.60 (Sintonen, 2000). Moreover, the trend in Figure 4.8b is the large difference (EF_{max} – EF_{min}), which spans from 0.43 in May to 0.88 in September, indicating already, more or less, the poor accuracy of the generated evaporative fraction. This underestimation of evaporative fraction is likely to influence the output of daily evaporation, which could also be in turn underestimated.

4.3.2. Daily evaporation (DE)

Plate 3b shows the map of daily evaporation for July 14th 2003 as derived from the NOAA image. From this map, we can identify some spots of values between 0 and 1 mm/day in the western part of the Netherlands, some spots of 2.5 to 3 mm/day in the northern part and in the inter land water body. The major land and the Noordzee have values from 1 to 2 mm/day of evapotranspiration.

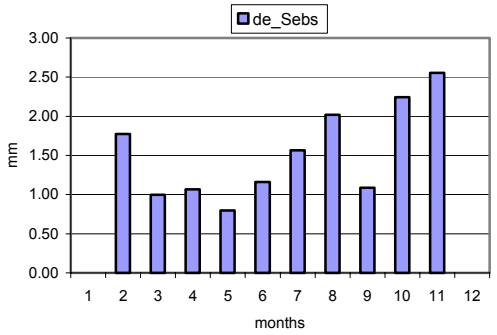

Figure 4.9a: Graph of mean DE values over 15 years

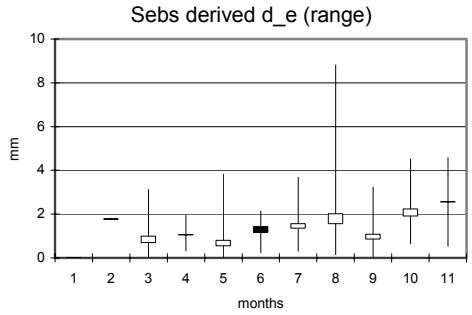

Figure 4.9b: SEBS_DE range values over 15 years

Table4.9: Summary statistics of monthly DE values over 15 years.

month	Measure of location				spread	shape	
	max	min	mean	median	st.dev	CV	skew
Jan	-	-	-	-	-	-	-
Feb	1.81	1.74	1.77	1.77	0.05	0.03	
Mar	3.13	0.01	1.00	0.68	0.97	0.97	1.23
Apr	1.95	0.33	1.07	1.04	0.47	0.44	0.32
May	3.83	0.01	0.80	0.54	0.99	1.24	2.75
Jun	2.13	0.24	1.16	1.44	0.59	0.51	-0.16
Jul	3.68	0.30	1.57	1.35	1.01	0.64	1.15
Aug	8.82	0.15	2.02	1.55	2.10	1.04	2.92
Sep	3.23	0.03	1.09	0.85	1.02	0.93	0.95
Oct	4.52	0.64	2.24	1.90	1.85	0.83	0.55
Nov	4.58	0.53	2.55	2.55	2.87	1.12	
Dec	-	-	-	-	-	-	-

The variability of the monthly evaporation values averaged over the 15 years is illustrated in Figure 4.9a. The daily evaporation has not a normal distribution and even decreases in May where it is expected to increase and it increases in November where it is expected to decrease. This overall trend is abnormal and is the result of an underestimation, which

might be figured out in the validation process. This trend is illustrated once again in the graph of range values (Figure 4.9b). The table of summary statistics confirms this one more time with an overall high CV value. The skewness coefficients also show a tail of high erratic values, as a result of a few high values among a large number of low values that lowered the overall mean. This unexpected underestimation should be highlighted by validation and the investigation of understanding what went wrong in SEBS processing.

4.4. Data validation and discussion

To understand the meaning of the SEBS output results and its relevancy, a data validation part was carried out in this project. In that respect, we successively examined the main remote sensing input parameters (Albedo, land surface temperature and NDVI), its magnitude through its distribution and the expectation for the Netherlands. Afterwards, we have a look at the energy partitioning and compare the net radiation derived by SEBS with the measured KNMI global radiation. The difference between the two and its effect on daily evaporation is discussed while comparing SEBS derived daily evaporation with the KNMI measured one.

4.4.1. Validation of input remote sensing data

- Surface albedo

There are no station-measured values of certain type of the input data like albedo and NDVI used in this study. But expert knowledge can help us to closely have a look at these parameters and understand their meaning. Figure 4.1a shows the estimated trend of albedo for the Netherlands. One may notice the relatively high values in March, April, September and October (albedo≥ 30%) along with relatively low values from May to August (albedo≤18.5%). In fact, for the growing season, one might expect the mean albedo to be around 23% (i.e. 20%<albedo<25%). These values are used in the parameterization of the net radiation (energy input for evaporation) by KNMI (the Makkink method) and FAO (De Bruin & Stricker, 2000). The observed values of albedo in wintertime are too high and might be explained by cloud cover or snow effects on the NOAA image of that period of the year.

- Land surface temperature

On a station basis, KNMI measures the soil temperature at 10cm below the surface. In this study without any surface temperature measured by KNMI, we use that temperature at 10cm below the surface as the KNMI measured land surface temperature to "validate" the SEBS derived land surface temperature from the preprocessing of NOAA data in combination with KNMI measured air temperature (T_a). Although the KNMI data are point measurements, its comparison with SEBS large-scale data has the merit to give an indication of how good our SEBS output for this parameter is. This is particularly true (while rely on the KNMI temperature records for air temperature, soil temperatures at 10cm and 150cm under the ground and their spatial repartition over the country) since there are no big differences between the air temperature and the soil temperature at 10cm below the surface for the Netherlands.

Figure 4.10a to c show respectively the graph of KNMI and SEBS land surface temperature, the difference SEBS minus KNMI and the regression line of SEBS data explained by KNMI. In general, SEBS overestimates the land surface temperature compared to KNMI measurements, i.e. $T_{SEBS}>T_{KNMI}$ (Figure 4.10a). The difference, SEBS minus KNMI, rises up to 8°C in June (Figure 4.10b). This trend has the negative effect of increasing the difference of SEBS surface temperature minus air temperature (T_s-T_a) used in the sensible heat flux estimation since the latter is directly proportional to the former (cf. eq. 2.5).

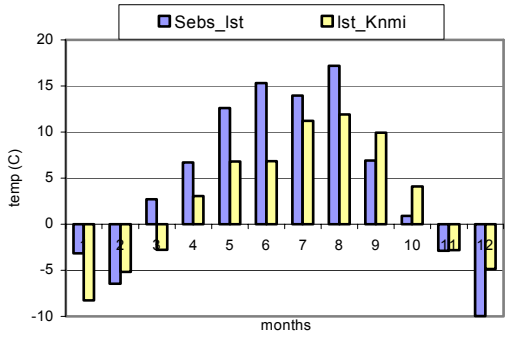

Figure 4.10a: Graph of lst (SEBS & KNMI) values over 15 years

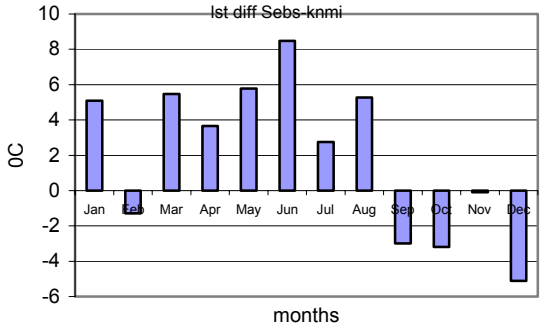

Figure 4.10b: lst difference (SEBS-KNMI) values over 15 years

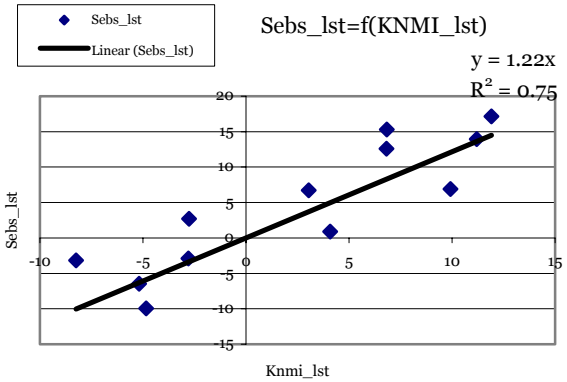

Considering the air temperature (T_a) as a constant input, T_{SEBS} - T_a will be larger than T_{KNMI}-T_a because $T_{SEBS}>T_{KNMI}$. Then one understands why the assessment of that difference is an important factor to give a clue to explain the sensible heat values later. In a normal situation, the difference (T_s -T_a) is very small. Due to this drawback effect enumerated above, the SEBS method will then generate a poor accuracy of the sensible heat flux and affect the evaporation estimation by lowering its values. The regression line of SEBS_lst as a function of KNMI_lst forced by the origin of the axes (Figure 4.10c) has a slope of 1.22 (bigger than 1) and an R^2 of 75% where the expectation is 100% (i. e. should fit perfectly to the 1:1 line). This confirms again the overestimation of the SEBS method for the land surface temperature estimation.

- NDVI

The graph of Figure 4.3a shows the distribution of NDVI averaged values over the year. At first view, the trend shown is quite normal for the Netherlands. But when we consider the importance of NDVI for emissivity estimation, the emissivity as input for the land surface temperature, and all three together as inputs for available energy partitioning, the accuracy required for NDVI must be high. A slight error in NDVI is propagated all over the processing and accumulates to end up with a huge error. Information on the accuracy of our used NDVI values would have been checked, if compared with the actual in-situ measurements, which we do not have. Nevertheless, we try to assess how spatially accurate our NDVI is by computing it on a station basis and comparing it with the overall image basis. Figure 4.11a shows a computed NDVI of 100 pixels around each of the six (6) main stations used by KNMI compared with the NDVI of the whole image for the year 2003.

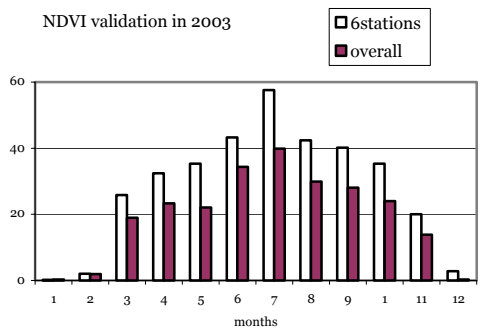

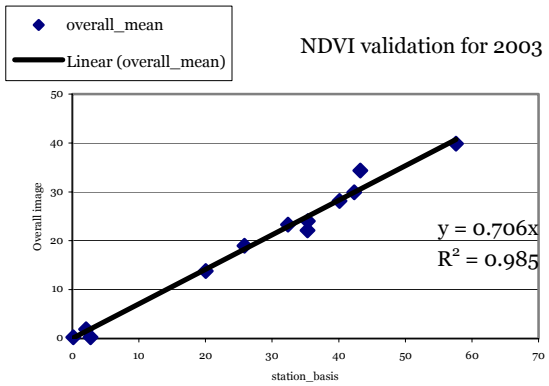

Figure 4.11b is the linear regression forced through the origin of the whole image values as a function of that of the station based computations and it has a slope of 0.706 (< 1), thus this indicates an overall underestimation of NDVI for the whole image basis compared to per station basis. Although the R^2 is 98%, the result is biased and we shouldn't take that fact for our analysis. The analysis based on the slope, which indicates an underestimation of NDVI at image basis, is illustrated and reconfirmed in the monthly relative difference shown in Table 4.10. From that table, during the growing season, the relative spatial difference between the NDVI values of the image basis and that of the per station basis goes from a minimum of 20.47% (in June) to a maximum of 37.47% (in May). These spatial differences observed between image basis and per station basis of NDVI values can be explained by the composite of land use units that made up the whole country. Thus NDVI values on an image basis have a smoothing effect compared to per station basis. In that respect, it might be important in the near future to reconsider the contribution of NDVI in energy computation and partitioning in the SEBS method if we would like to promote that method for the evaporation estimation at a large scale to the detriment of the conventional point measurement method used by KNMI.

Table4.10: NDVI spatial difference in 2003

Month in 2003	min	max	st dev	6stations _mean	overall_ mean	relative difference(%)
Jan	0.00	4.85	0.79	0.15	0.28	-86.67
Feb	2.05	2.09	0.00	2.06	1.93	6.39
Mar	11.10	38.68	6.42	25.85	18.95	26.70
Apr	15.36	44.26	6.77	32.39	23.33	27.97
May	17.38	45.01	5.93	35.33	22.09	37.47
Jun	23.14	57.99	7.94	43.23	34.38	20.47
Jul	34.00	67.46	7.33	57.60	39.85	30.81
Aug	20.50	51.85	6.39	42.34	29.94	29.29
Sep	18.78	53.17	7.36	40.12	28.11	29.93
Oct	14.07	48.79	7.40	35.34	24.04	31.97
Nov	9.40	24.75	3.77	20.03	13.80	31.09
Dec	0.00	6.51	1.45	2.76	0.29	89.49

This illustrates one of the main origins of errors in the SEBS computation to derive daily evaporation along with the surface roughness (z_o), the surface resistance (r_s) and the aerodynamic resistance (r_a) parameters to be discussed later.

4.4.2. Validation of energy balance terms

The available energy at the earth surface is split into ground heat flux, sensible heat flux and latent heat flux at certain proportions according to the meteorological and surface state of the earth. As part of the validation process, we first attempt to measure the proportion of each flux from the net radiation per month. That is the internal validation. Then follows the external validation where SEBS derived net radiation is compared to KNMI measured global radiation.

- Internal validation of R_n partitioning

Figure 4.12a to Figure 4.12d show respectively the monthly net radiation mean value over the 15 years study period (Figure 4.12a), the subdivision into latent, sensible and ground heat fluxes (Figure 4.12b), the comparison of net radiation and the sum (G+H+λE) radiation (Figure 4.12c) and the proportion of each flux into net radiation (Figure 4.12d).

The comparison between graphs Figure 4.12a and Figure 4.12b shows their similarity and describes the same trends and shapes. This is to say that the net radiation is equal to the sum of ground, sensible and latent heat fluxes at the earth surface that is termed surface energy balance. The matching of these two figures is illustrated again in the graph of Figure 4.12c. The differences between the sum and the net radiation observed in April, May, August and September are small and might be related to small uncertainties and are not of a nature to generate high errors at a later stage.

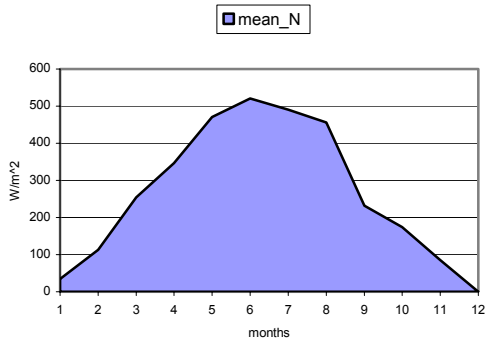

Figure 4.12a: Mean Rn values over 15 years

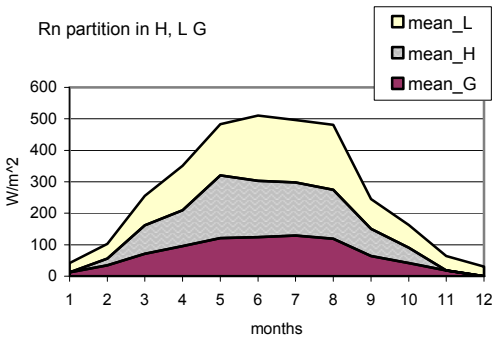

Figure 4.12b: Contribution of Go, H and LE into R_n over 15 years

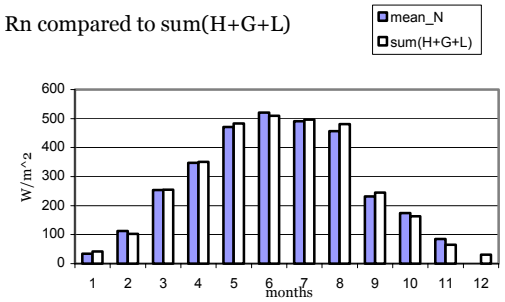

Figure 4.12c: Rn compared to sum(G+H+L)

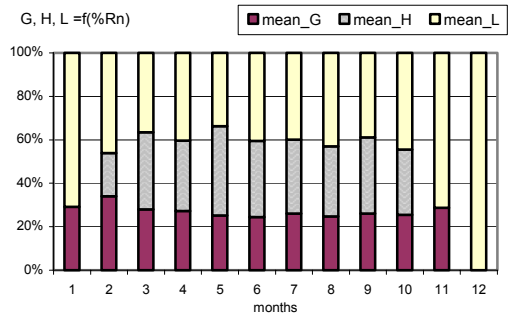

Figure 4.12d: Proportion of Go, H and LE into R_n over 15 years

Figure 4.12d shows how much each flux contributes to net radiation over 15 years. This partition is of extreme importance for evaporative fraction calculation. Any mistake incorporated in this partition generates a systematic error of daily evaporation. Table 4.11 shows each proportion for each component of the net radiation.

De Bruin & Stricker (2000) found good evaporation estimates for grass in the Netherlands with the formula $\lambda E = 0.86(R_n - G_o)$ and stated that during the growing season, G_o is often small compared to R_n. Starting from that result, one can expect not only in grassland but over a cosmopolite area of composite land use units up to 75% of R_n partitioning into latent heat, 20% of R_n into sensible heat and 5% into ground heat flux. That is not the case shown by our results in Table 4.11. There is an overestimation of ground heat flux at the cost of an underestimation of latent heat flux. Probably this is prompt to induce great underestimation of daily evaporation.

Table 4.11: Proportion of Go, H and λE into Rn

months	G=f(%Rn)	H=f(%Rn)	λE=f(%Rn)
Jan	35.33	-	86.02
Feb	31.06	18.14	42.00
Mar	28.09	35.70	36.69
Apr	27.52	32.87	40.74
May	25.79	42.15	34.56
Jun	23.88	34.38	39.69

Jul	26.31	34.42	40.43
Aug	26.06	34.00	45.41
Sep	27.54	37.16	41.05
Oct	23.85	28.32	41.69
Nov	21.66	-	53.94
Dec	-	-	-

- External validation of R_n with KNMI measured data

The SEBS derived net radiation internally validated might be checked against an external measurement to be sure of none existence of other sources of error in our process. This external measurement is offered by KNMI that measured an average daily incoming global radiation. The graph of Figure 4.13a shows the comparison of R_n as derived by SEBS with the daily average KNMI measured global radiation.

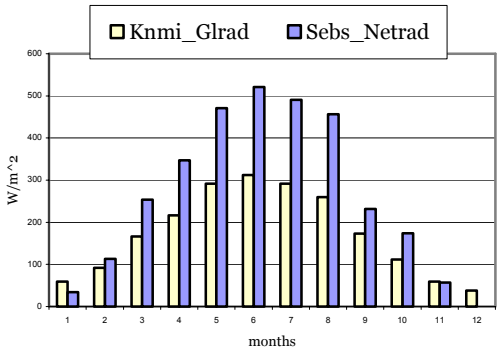

Figure 4.13a: R_n validation with KNMI measurements over 15 years

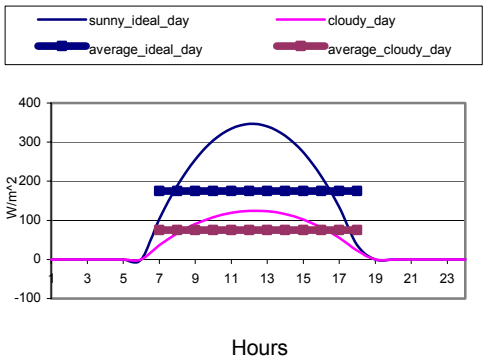

Figure 4.13b: Simulation of daily net radiation variation

To be able to fully understand both graphs, it is important to explain the difference in denomination of both terms: net radiation (SEBS) and global radiation (KNMI). The amount of energy from the sun reaching the top of atmosphere is termed in SEBS terminology as global energy from which part will be reflected back by the atmosphere and its constituents (gas and dust). The remaining of that energy reaches then the earth surface, and after reflecting by the surface, is available energy for all processes and life on the earth. That is what is termed as "Net radiation" in SEBS. That net radiation is made up of energy from both short wavelength and long wavelength radiation. The equipment of KNMI is able to measure only the incoming short wavelength radiation and that is what KNMI termed "Global radiation". In summary, the KNMI measurement is part of the SEBS estimated net radiation. This explains clearly that SEBS derived values should be greater than KNMI measured data, as shown by Figure 4.13a. Both

graphs have the same trends and shape; and the differences shown are bigger during the growing season (March to October). The explanation is that it comes more long-wave radiation during that period of the year but the magnitude of the observed difference might not be described only by the incoming long-wave radiation. KNMI values show the mean over the day (thick and horizontal lines in Figure 4.13b), so they are constant for the whole day, where SEBS is a point measurement along the parabolic shape variation values (fine curved lines). Depending on the atmospheric condition of a day (sunny day or not; cloudy day or not etc.), both methods can show high or low values.

To summarize this section of net radiation external validation, one can say that the SEBS derived values of this parameter are in the good range for the Netherlands and the distribution over the year seems normal with the maximum of nearly 600 W/m² around June.

4.4.3. Daily evaporation validation

The ultimate objective of this work is the estimation of the daily evaporation over the Netherlands and its behavior during the 15 years study period (see graphs of appendix 5b). The evaporative fraction, as final step before the daily evaporation, is defined as the ratio of latent heat (λE) over the available energy (H + λE). In the KNMI database, there is no measurement of latent heat flux that through validation one can be sure of having an accurate basis for daily evaporation. Nevertheless, we assessed this validation in section 4.3, where we discussed the fitting and correlation of the generated values of evaporative fraction along with daily evaporation. We pointed out already the general trend of lower values and the large variability it contained. Here comparison is made of SEBS derived daily evaporation with KNMI measured daily evaporation. The graph of Figure 4.14a shows the general relationship between the two. In general, the SEBS values are smaller than the KNMI derived ones with the lowest value in May. Even the computation of the daily evaporation mean value over 100 pixels around each of the six (6) main KNMI stations (shown as de_Sebs_6 in Figure 4.14a) does not improve significantly our results. This is not surprising because all the input parameters were those of the whole image of the Netherlands, each of which is with its own drawback features described and discussed in the previous sections.

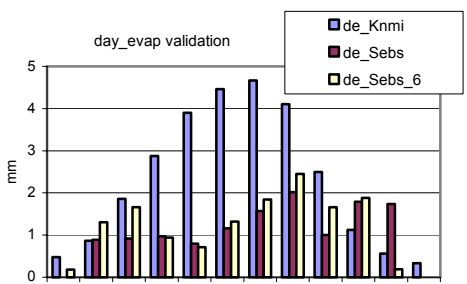

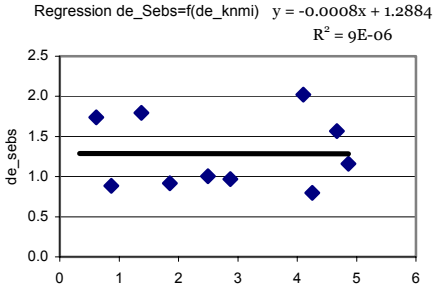

If the computation results were good in general, one might expect a normal distribution shape as the one of KNMI data shown in Figure 4.14a. The state of none correlation between the two dataset is shown by the regression line with a slope of 0 and an R^2 almost zero (Figure 4.14b).

4.4.4. Specific validation with Sintonen's findings

Before us, Sintonen *et al.* (2002). used data of 1995 in the SEBS along with field measurements data at Cabauw and Speulderbos sites to derive evaporative fraction for the Netherlands. This gave us the opportunities to compare our outputs with her results. These opportunities are even greater since we were able to access her output image files. The three remote sensing derived input data, namely albedo, land surface temperature and NDVI were computed over the whole country while the energy balance terms with the evaporative fraction were computed on sample image data of about 50*33 = 1650 pixels taking her images as input for resized data around the sites (region of interest). The computed values along with the graphs are in appendix 6. In general our results look like her results. The SEBS inputs albedo, land surface temperature and NDVI are of the same shape with an overestimation of albedo in wintertime (October to December) and a relatively small underestimation of surface temperature for our results. The net radiation is in general slightly underestimated except for June and July where our results are bigger than hers. The big discrepancies are found in latent heat and sensible heat graphs. However, the soil heat fluxes in both results match each other. Overall the same trends of the evaporative fraction are observed and one can confirm the poor performance of SEBS from June to August and erratic results in winter (> 100%). Unfortunately she didn't assess the daily evaporation values so we couldn't compare those parameters. All things remaining equal in addition, one can expect comparable results as regards the daily evaporation if it was also calculated.

4.5. Partial conclusion

After having a global look at the different parameter outputs and discussing them in detail, we can make a resume of all the processing with a background of all formulas used in chapters 2 and 3 of this thesis. In general, albedo is an input parameter for energy partitioning and evaporative fraction calculation in only one step of the process. The discussion of section 4.1.1 concludes that the expected error due to albedo would be small. The land surface temperature parameter is generated after use of the emissivity derived by NDVI. All four of them (albedo, emissivity, land surface temperature and NDVI) are input parameters for energy partitioning and evaporative fraction calculation. Thus at its own, NDVI counts for three (3) levels of input parameters i.e. as much opportunities for error accumulation. In addition, NDVI is used as a surrogate for LAI calculation and vegetation coverage fraction in soil heat flux parameterization. That shows clearly that NDVI is a crucial parameter in SEBS processing. For our case, the section about NDVI validation (section 4.4.1) points out clearly that more than 20% of the information is lost when use is made of the overall NDVI values as SEBS did during the growing season. 20% lower NDVI values have generated a very poor result in energy partitioning, namely an overestimation of ground heat flux and an underestimation of latent heat flux.

When looking backward to see what can explain the error in NDVI, one may consider the external aerodynamic resistance function of surface roughness. While working with a relatively large area like the Netherlands, where the surface meteorological parameters and the surface geometrical and thermal conditions are neither constant nor homogeneous, special attention must be given to the surface roughness and aerodynamic resistance parameter. There lies the main explanation of our poor results. Furthermore, comparison with KNMI measured data (local scale measurements aggregated for a certain number of stations to get a value for the Netherlands) might not always be direct and of 1 to 1 correspondence. So, it can be concluded after Sintonen *et al.* (2002) that: ”The difficulty of estimating the aerodynamic surface variables using remote sensing techniques, the estimation of surface fluxes over heterogeneous landscapes consisting of a mix of low and high vegetation and urban areas remain a major challenge for the successfulness of the SEBS algorithms”.

CHAPTER 5: General conclusionS and recommendations

The application of the Surface Energy Balance Systems (SEBS) with remote sensing techniques on NOAA data in combination with meteorological data is used to derive a long-term evaporation data set for a large scale. The results, without being fully satisfactory since they do not match the KNMI measurements, are still promising if some improvements are made for future uses. Specific conclusions, relevant for this work and which explain our results, are as follows.

5.1. Conclusions

(1) Fulfilling objective (i) and answering research question (i): One can say that SEBS yielded good net radiation estimation, but did not perform satisfactorily at its partitioning step. In fact a large weight was being giving to soil heat and sensible heat fluxes at the cost of latent flux. The overestimated surface temperature and underestimated NDVI explain this poor partitioning of the net radiation at the soil surface. If well performed, an accurate net radiation partitioning can lead to a good estimation of the daily evaporation for the Netherlands.

(2) Fulfilling objective (ii) and answering related research question: A poor correspondence is found between KNMI measured and SEBS derived daily evaporation. Only 12 days out of 145 computed ones match each other. That big discrepancy finds its explanation in the weak net radiation partitioning which in turn might be explained by the preliminary and intermediary input results.

(3) Fulfilling objective (iii) and answering related research question: The parameterization of the soil heat and the sensible heat fluxes relies heavily on input data like NDVI, soil temperature, albedo and surface aerodynamic parameters (wind speed, roughness height, stability correction functions). Our results show an underestimation of NDVI and an overestimation of land surface temperature, resulting in a propagation and accumulation of errors from these parameters along the processing together with those of the inadequate stability correction functions (Su, 2000). That explains the poor performance of SEBS in

the energy partitioning and as a result the poor accuracy of the daily evaporation. That illustrates the sensivity of the daily evaporation to all these input data.

(4) Fulfilling objective (iv) and answering related research question: With these results, one can be convinced that a good energy partitioning will lead to precise daily evaporation estimation through SEBS. Once a daily estimation is obtained, one can go forward to monthly, seasonally or yearly evaporation estimation or backward to hourly evaporation estimation.

Moreover, the following factors can also, at certain extent, explain our results:

(5) Differences in atmospheric conditions from day to day are not included in the empirical values used for water vapor and reference height, and those empirical fixed values can cause systematic errors in the retrieved land surface parameters.

(6) For this study, we have neither tower measurements nor radio sounding data for the aerodynamic surface variables and PBL variables such as the potential temperature and potential pressure, wind speed. So, their used values are questionable.

(7) The computational processing involves many steps wherein input data (like NDVI) are used and reused. The error will be transferred and accumulated from step to step in such a way that the error at the end becomes significant.

(8) Atmospheric conditions are *a priori* neither stable nor constant over the whole pixel of a lower resolution NOAA image (1100 m) and so they are, *a fortiori,* for the whole Netherlands. That means that the used mean values of surface temperature, pressure or wind speed bore already uncertainties or errors. Furthermore, a larger pixel of lower resolution images reflects a combination of varieties of land use units with various properties. So, the generated average values of NDVI or albedo per pixel are *a priori* with uncertainties.

SEBS does not need a priori knowledge of the actual turbulent heat fluxes and thus is considered as an independent approach (Su, 2002). That credibility and independency

will be increased, and the generated results will become more reliable, if some improvements are made. Then we consider the following recommendations as important factors that may help in improving the user guide of the SEBS processing and yield more reliable results.

5.2. Recommendations

(1) SEBS can be improved through a better parameterization. That is the task of future research under different climate conditions like tropical, mediterranean and mid-latitudes. The calibration and parameterization of all the processing has to be checked again to be sure that prerequisites are satisfied in net radiation and soil heat flux calculation and to avoid an overestimation of soil heat flux at the cost of sensible and latent heat fluxes.

(2) As prerequisites, much care has to be given to the PBL parameters derivation, especially while using SEBS for larger areas like a country. Moreover, the location might be taken into account like mid-latitude, tropical areas or Mediterranean areas as zone of interest. These requirements are important since PBL parameters are sensitive to latitudes.

(3) The importance and role of the meteorological visibility has to be reviewed to fulfill the requirement in the SEBS procedure. At least a clear way of conversion from station measurement to input for SEBS has to be defined.

(4) The map projection used during SEBS processing has to be set in such a way that each user can choose for the projection suitable for his area of interest.

(5) Although it is not suitable for large scale studies, the use of higher spatial resolution images like LANDSAT or MODIS for surface parameter retrieval can improve the accuracy of the derived results like albedo, land surface temperature and NDVI, and further improve SEBS derived evaporation especially for local studies.

References

Brutsaert, W., 1982. Evaporation into the atmosphere. D. Reidel, 299pp.

Caselles, V. and Sobrino, J.A., 1989. Determination of frosts in orange groves from NOAA-9 AVHRR data. *Remote Sens. Environ.*, **29**, 135-146.

Coll, C. and Caselles, V., 1997. A split window algorithm for land surface temperature from AVHRR data: validation and algorithm comparison. *Journal of Geography Research*, **102**(**14**), 16697-16713.

De Bruin, H.A.R., 1998. *Micrometeorologie*, Wageningen Universiteit, Vakgr. Meteorologie, 156pp.

De Bruin, H.A.R. and Stricker, J.N.M., 2000. Evaporation of grass under non-restricted soil moisture conditions. *Journal of Hydrological Sciences.,* **45**(3), 391-406

Isaaks, H.E. and Srivastava, R.M., 1989. An introduction to Applied Geostatistics. Oxford University press, 561pp.

Jackson, A.R.W. and Jackson, J.M., 1998. The natural environment and human impact. In: *Environmental Science*, Longman Group Limited (Eds.).UK. 1996. 370pp.

Kustas, W.P. and Daughtry, C.S.T., 1989. Estimation of soil heat flux/net radiation ration from spectral data. *Agr. Forest. Meteorol.,* **49**, 205-223.

Li, X., 2001. Estimation of Urumqi river basin evaporation with remote sensing. MSc thesis IHE Delft.82 pp.

Massman, W.J., 1997. An analytical one-dimensional model of momentum transfer by vegetation of arbitrary structure. *Bound-Lay. Meteorol.*, **83**, 407-421.

Massman, W.J., 1999. A model study of kB^{-1}_{H} for vegetated surfaces using 'localized near-field' Lagrangian theory. *J. Hydro.*, **223**, 27-43.

Monteith, J.L., 1973. *Principles of environmental physics*. Edward Arnold Press. 241pp.

Owen, O.S., Chiras, D.D. and Reganold, J.P., 1998. Managing water resources sustainably. In: *Natural Resource Conservation*, 7th ed. Printice-Hall, Inc. USA. 594pp.

Rauwerda, J., Roerink, G.J. and Su, Z., 2002. Estimation of evaporative fractions by the use of vegetation and soil component temperatures determined by means of dual-looking remote sensing. *Alterra Green World Research, Wageningen,* Alterra-report **580**. ISSN 1566-7197. 148pp.

Sintonen, K.H. Su, Z. and Wen, J., 2002 The surface energy balance system (SEBS): Validation using field data from the Netherlands. *Alterra Green World Research Wageningen*, 44pp.

Stull, R.B., 1999. *An Introduction to boundary Layer Meteorology*, Kluwer academic Publishers, Dordrecht The Netherlands, ISBN 90-277-2768-6. 669pp.

Su, Z., 2000. Remote sensing of land use and vegetation for mesoscale hydrological studies. *Int. J. Remote Sens.*, **21**, 213-233.

Su, Z., 2001. A surface Energy Balance System (SEBS) for estimation of turbulent heat fluxes from point to continetal scale, In: *Advanced Earth Observation – land Surface Climate,* Z. Su and

Jacobs, C. (Eds.) 2001. Publication of the National Remote Sensing Board (BCRS), USP-2, 01-02. 184pp.

Su, Z., 2002. The surface Energy Balance System (SEBS) for estimation of turbulent hat fluxes. *Hydrology and Earth System Sciences*, **6(1)**, 85-99.

Su, Z., Menenti, M., Pelgrum, H., van den Hurk, B.J.J.M. and Bastiaanssen, W.G.M., 1998. Remote sensing of land surface fluxes for updating numerical weather predictions. In: *Operational Remote Sensing for Sustainable development,* G.J.A. Nieuwenhuis, R.A. Vaughan and M. Molenaar (Eds.). Balkema, The Netherlands. 393-402.

Su, Z., . Wen, J. and. Wan, L. 2001a. A methodology for the retrieval of land physical parameters and actual evaporation using NOAA/AVHRR data. *Journal of Jilin University (Earth Science Edition)*, **33(sup.),** 106-118.

Su, Z., Schmugge, T., Kustas, W.P. and Massman, W.J., 2001b. An evaluation of two models for estimation of the roughness height for heat transfer between the land surface and the atmosphere. *J. Appl. Meteorol.* **40**, 1933-1951.

Su, Z., Yang, Y., Zhang, J., Lu, G., Zhou, G., Roerink, G.J., Qi, J., Liu, J. Wang, L., Wen, J., Jia, L., Zheng, W., Yue, Z. and Chen, X., 2003a. A technique for large scale drought monitoring. *Alterra Green World Research, Wageningen,* Alterra-report **683**. ISSN 1566-7197. 88pp.

Su, Z., A. Yacob, Y. He, H. Boogaard, J. Wen, B. Gao, G. Roerink, and K. van Diepen, 2003b, Assessing Relative soil moisture with remote sensing data: theory and experimental validation, *Physics and Chemistry of the Earth*, **28(1-3),** 89-101.

Valiente, J.A., Nunez, M., Lopez-Baeza, E. and Mereno, J.F., 1995. Narrow-band to broad-band conversion for meteosat-visible channel and broad-band albedo using both AVHRR-1 and –2 channels. *Int. J. remote Sens.*, **16(6)**, 1147-1166.

Wieringa, J., 1986. Roughness-dependent geographical interpolation of surface wind speed averages. *Quart. J. Roy. Meteorol. Soc.,* **112**, 867-889.

Wieringa, J., 1993. Representative roughness parameters for homogeneous terrain. *Bound-Lay. Meteorol.,* **63**, 323-363.

Web pages (date of first visit)

www.knmi.nl/product (08/06/2003)

www.saa.noaa.gov (08/06/2003)

http://www.arm.gov/docs/sites/sgp/news/sgpfacility/oct00.pdf (29/07/2003)

http://faldo.atmos.uiuc.edu/w_unit/LESSONS/water.cycle.html (19/08/2003)

http://users.rcn.com/jkimball.ma.ultranet/BiologyPages/T/Transpiration.html (19/08/203)

http://edcdaac.usgs.gov/gtopo30/hydro/europe.html (15/12/2003)

http://hurri.kean.edu/~yoh/calculations/satvap/satvap.html (23/12/2003)

http://hurri.kean.edu/~yoh/calculations/moisture/Equations/moist.html (23/12/2003)

http://members.aol.com/Accustiver/wxworld_calc.html . (23/12/2003)

http://hurri.kean.edu/~yoh/calculations/diagnostic/diagnostic.html (23/12/2003)

http://www.srh.noaa.gov/ffc/html/gloss1.shtml (24/01/2004)

APPENDICES